2nd4

Final Report of Research Performed Under NASA Grant NGR 36-028-006,

Covering the Period 9/1/72 - 11/30/73

Submitted to the

National Aeronautics and Space Administration

By

Youngstown State University, Youngstown, Ohio 44503

"APPLICATION OF ULTRASONIC SIGNATURE ANALYSIS FOR FATIGUE DETECTION IN COMPLEX STRUCTURES"

Principal Investigator: Allan Joseph Zuckerwar
Assistant Professor
Electrical Engineering

NASA Technical Officer: David L. Gray
Structural Mechanics Instrumentation Section
Instrument Research Division
NASA - Langley Research Center

Personnel: Kin-Ping Moy
Graduate Research Assistant

Date of Submission: February 28, 1974

APPLICATION OF ULTRASONIC SIGNATURE ANALYSIS FOR FATIGUE DETECTION IN COMPLEX STRUCTURES

ABSTRACT

Ultrasonic signature analysis shows promise of being a singularly well-suited method for detecting fatigue in structures as complex as aircraft. The method employs instrumentation centered about a Fourier analyzer system, which features analog-to-digital conversion, digital data processing, and digital display of cross-correlation functions and cross-spectra. These features are essential to the analysis of ultrasonic signatures according to the procedure described here. In order to establish the feasibility of the method, the initial experiments were confined to simple plates with simulated and fatigue-induced defects respectively. In the first test the signature proved sensitive to the size of a small hole drilled into the plate. In the second test, performed on a series of fatigue-loaded plates, the signature proved capable of indicating both the initial appearance and subsequent growth of a fatigue crack. In view of these encouraging results it is concluded that the method has reached a sufficiently advanced stage of development to warrant application to small-scale structures or even actual aircraft.

APPLICATION OF ULTRASONIC SIGNATURE ANALYSIS FOR FATIGUE DETECTION IN COMPLEX STRUCTURES

I. INTRODUCTION

The research into ultrasonic signature analysis initiated under NASA Grant 36-028-006 has the following consecutive objectives:

(1) An immediate objective, to establish ultrasonic signature analysis as a practical method of detecting flaws and fatigue in structural components

(2) An ultimate objective, to develop a system of instrumentation for the purpose of utilizing ultrasonic signature analysis as a supplement to present methods of inspecting aircraft in the field.

The instrumentation centers about a Fourier analyzer system, such as the Hewlett-Packard Model 5451A, which features analog-to-digital conversion, digital data processing, and digital display of cross-correlation functions and cross-spectra (ref. 1). These features are essential to the analysis of ultrasonic signatures as described in this report.

In contrast to other methods of nondestructive fatigue detection, ultrasonic signature analysis shows promise of being singularly suited for application to structures as complex as aircraft, in which many structural components are inaccessible to visual inspection. At present fatigue detection in these structures is limited primarily to visual and dye-check methods. If during a routine phase inspection a part of the structure is suspected of having suffered fatigue damage, then cracks are sought by means of a conventional nondestructive method, for example the ultrasonic pulse-echo, magnetic rubber inspection, eddy current, or X-ray method. In

principle, the ultrasonic signature instrumentation could be applied by an operator directly to the structure and the results obtained within a few minutes. The findings would be used to supplement those obtained by other methods and may even provide additional information.

A system for detecting fatigue in aircraft must be capable of fulfilling three basic requirements:

(1) Adaptability to complex structures. The system must lend itself to interrogating extensive regions of a large structure, even if the structural components provide irregular and contorted paths. By several methods - notably eddy current, X-ray, and to a lesser extent ultrasonic pulse-echo - the interrogation is confined to small local regions of the structure. These regions may be extended by scanning, but scanning is time-consuming, requires elaborate accessory equipment, and reduces sensitivity. Other methods, such as ultrasonic imaging and holography, which require the structure to be immersed in a liquid, may certainly be ruled out as unsuited for aircraft.

(2) Ample depth of interrogation. The system must be capable of detecting cracks and other flaws well within the interior of the structure as well as on the surface. X-rays and magnetic rubber inspection, on the contrary, have limited depth of penetration.

(3) Large signal-to-noise ratio. A system whereby the structure responds to an externally introduced flux (electric, magnetic, ultrasonic, etc.) has a great advantage over one in which the structure generates its own response signal (acoustic emission) or remains passive (optical methods). Under external excitation enough power can be pumped into the structure to minimize problems concerning signal-to-noise ratio.

The system developed here for the practical realization of ultrasonic signature analysis is capable of fulfilling all three of the above requirements.

The experimental program is intended to proceed according to the following work phases, arranged in order of increasing complexity of the specimen tested:

Phase 1 - simple specimen with a simulated defect

Phase 2 - simple specimen with a fatigue-induced defect

Phase 3 - small scale model of an aircraft

Phase 4 - full-scale model or actual aircraft.

The goal of the first year is to complete Phases 1 and 2, and in doing so, to achieve the immediate objective of this investigation. Contingent upon the successful establishment of this groundwork, the goal of Phases 3 and 4 conforms to the achievement of the ultimate objective.

II. GENERAL DESCRIPTION OF ULTRASONIC SIGNATURE ANALYSIS

A. Principle of Operation

Let the source of ultrasound be a piezoelectric transducer, excited to transmit a standard ultrasonic signal throughout the structure under test. Receiving transducers, located at strategic positions on the structure, will respond to the ultrasound to produce a characteristic, generally complex electrical signal, which after processing provides the signature for the structure. The transducers may be mounted permanently to eliminate variations in coupling. The signatures are to be monitored after selected intervals of structural loading, each compared to its predecessor. Small changes in the structure, such as crack formation,

work hardening, plastic deformation, corrosion, loosening of joints, etc., will generally cause corresponding changes in the signature; for the propagation of ultrasound is extremely sensitive to the properties of the medium, as is well known.

An ultrasonic frequency near 10 MHz, corresponding to a wavelength of about 0.025 inch, is thought to be optimal for this application.[1] A wavelength of this order is much smaller than most of the linear dimensions of the structure (and of the same order as the skin thickness of wing and fuselage of most aircraft). Thus the ultrasonic signal will depict events taking place well within the interior of the structural components and will not depend so much upon surface conditions. Higher frequencies will not improve the signature because of increasing attenuation, which for most physical processes increases as the square of the frequency.

B. Possible Causes of Change in the Signature

Among the physical mechanisms which will affect the propagation of ultrasound and thus cause changes in the signature are those described below.

(1) Scattering by internal flaws. An internal flaw, constituting an inhomogeneity or abrupt change in the medium, will scatter part of the transmitted ultrasonic wave. Although the angular distribution of the scattered intensity will generally be described by a complex pattern, a sufficiently strong scattered signal directed toward the receiving transducer will be incorporated into the signature. Changes in the scattering

---

[1]The actual frequency used, however, turned out to lie near 6 MHz, corresponding to a wavelength of 0.040 inch, for reasons given in Section III-A.

center will ordinarily manifest themselves as corresponding changes in the received signal and thus as changes in the signature.

(2) Diffraction by long cracks and large obstacles. Cracks much longer than the wavelength of the ultrasound, as well as other large obstacles as bolts, rivets, welds, ribs, and stringers, etc., will diffract rather than scatter the ultrasound. The diffraction pattern will be sensitive to changes in the size of the crack and to changes in the contact area between an obstacle and the medium.

(3) Harmonic generation. Under repeated loads certain regions of a structure, as a result of plastic deformation and work-hardening, may exhibit a nonlinear relationship between stress and strain. An ultrasonic wave of given frequency propagating through these regions will generate waves of higher harmonic frequencies (ref. 2). A system could conceivably use the harmonic content as an indication of the physical state of the medium along the propagation path of the ultrasonic wave.

(4) Absorption of ultrasound by defects. The application of stress to a material of such magnitude that the shear stress exceeds a critical value results in generation of dislocations, which, when present in sufficient quantity, cause considerable absorption of ultrasound. The Granato-Luecke theory of dislocation damping (ref. 3) predicts that the absorption will vary inversely with the square of the ultrasonic wavelength and directly with dislocation density, which in turn increases strongly with loading. As repeated loading of the structure continually increases the dislocation density of the affected regions, the accompanying loss of ultrasonic intensity at the receiving transducer may be noticeable in the signature.

(5) Mode conversion. If an ultrasonic wave incident upon an inhomogeneity or acoustical boundary is compressional, then, except under special circumstances, the refracted and reflected waves will have shear as well as compressional components. The generation of refracted and reflected shear waves from an incident compressional wave (or vice versa) is known as "mode conversion" (ref. 4). If the transmitting transducer is compressional, then the signal at a receiving shear transducer will be attributable in its entirety to mode conversion and may make a significant contribution to the signature.

(6) Reflection from boundaries. The amplitude of a reflected wave will be highly sensitive to changes in boundary conditions. For example, the appearance of a crack at an interior or exterior boundary could disperse a reflected wave to such an extent that the existence of the wave is no longer discernible at a receiving transducer.

(7) Shift in phase between transmitted and received signals. A change in sound velocity or path length between the transmitting and receiving transducers will shift the phase between the carrier components of the two signals. If the electronic system is sensitive to this phase shift, then the latter may play an essential role in the signature.

Several of these mechanisms have been found operative in changing the signatures obtained in the course of this investigation.

C. The Nature of the Signature

In order to gain some insight as to the type of signal we should expect at the receiving transducer, let us consider the simple scheme of figure 1. For the purpose of illustration let the ultrasound reach the receiving transducer R from the transmitting transducer S by way of

four different paths: Path 1, representing the "direct" path; Path 2, scattering from a flaw; Path 3, reflection from an obstacle; and Path 4, reflection from an exterior boundary. To discriminate between the various paths, the transmitted signal is amplitude-modulated by a sequence of periodic pulses of duration t_w and repetition interval T_o, as shown in figure 2(a). The effects of the pulse are noted at the receiver after times t_1, t_2, t_3, and t_4, the transit times over the four paths, respectively, as shown in figure 2(b). The contribution of Path 2 to the receiver signal is highly idealized for two reasons. First, the relative height of the pulse is greatly exaggerated, for we may expect the ultrasound scattered by a small flaw toward the receiver to be but a minute fraction of that arriving over the other paths. Secondly, random noise and other incoherent contributions to the receiver signal are ignored, which could obscure the pulse possibly beyond recognition.

A marked improvement in the selectivity of the system can be realized through cross-correlation of the signal at the receiver with that at the transmitter (refs. 5 and 6). By this technique the effect of the signal from Path 2 can be better isolated from noise and other signals. A fast Fourier analyzer, such as the Hewlett-Packard Model 5451A, is ideally suited for performing the function of on-line cross-correlation. Because the frequency response of the instrument is limited to 100 kHz (dual-channel), it is necessary that the carrier be removed before the transducer signals are applied to the input of the instrument.

The cross-correlation between two periodic signals, $S(t)$ and $R(t)$, is defined as

$$\phi_{SR}(\tau) = \frac{1}{T_o}\int_{-T_o/2}^{T_o/2} S(t)R(t - \tau)dt \qquad (1)$$

where T_o is the period and τ the "delay" time. If $S(t)$ represents a transmitted pulse of height p_o and width t_w, and $R(t)$ one of the received pulses, attenuated to a height ηp_o $(\eta < 1)$ and retarded by a transit time t_R, then the cross-correlation between the two pulses is given by the following expressions (ref. 7):

$$\phi_{SR}(\tau) = \frac{\eta p_o^2}{T_o}(t_w - \tau + t_R) \quad \text{if} \quad t_R \leq \tau \leq t_R + t_w \tag{2a}$$

$$= \frac{\eta p_o^2}{T_o}(t_w + \tau - t_R) \quad \text{if} \quad t_R \geq \tau \geq t_R - t_w . \tag{2b}$$

This function represents an isosceles triangle of height $\eta p_o^2 \, t_w/T_o$, base $2t_w$, and apex location $\tau = t_R$. The cross-correlation triangle associated with each of the received pulses is shown in figure 2(c). Because the time signals $S(t)$ and $R(t)$ are periodic, then $\phi_{SR}(\tau)$ is also periodic and has the same period. A display of $S(t)$ and $R(t)$ over one period constitutes a "record;" a display of $\phi_{SR}(\tau)$ over the period is called a "cross-correlogram" (ref. 8).

The process of averaging a large number of cross-correlograms tends to eliminate random noise in the transmitted and received signals. In reference 6, p. 299, we find a calculation of the gain in signal-to-noise ratio, over that obtained without cross-correlation, for the case of a sinusoidal signal buried in noise and random sampling. A similar analysis for the present case, a periodic pulse and sampling at fixed intervals, yields the following gain in signal-to-noise ratio (the signal taken at the peak of the cross-correlation triangle):

$$G = 10 \log n - 10 \log\left(1 + \eta^2 p_o^2 / p_N^2\right) \tag{3}$$

where G = gain in signal-to-noise ratio (dB)

n = the number of records

p_N = the acoustical pressure corresponding to the electrical noise at the receiving transducer.

Equation (3) leads to the following conclusions:

(1) The number of records n must exceed $\left(1 + \eta^2 {p_o}^2/{p_N}^2\right)$ in order for there to be any gain at all. Thus cross-correlation is most advantageous when $\eta p_o/p_N$ is small.

(2) The gain in signal-to-noise ratio amounts to 10 dB per decade in n.

Using typical values $\eta p_o/p_N = 1$ and $n = 100$, we find

$$G = 10 \log 100 - 10 \log 2 = 17 \text{ dB}.$$

The Fourier transform of $\phi_{SR}(\tau)$, the "cross-power" spectrum, is given by the following expression for the case of a single received pulse (ref. 9):

$$G_{SR}(f) = \frac{\eta {p_o}^2 {t_w}^2}{{T_o}^2} \sum_{n=-\infty}^{\infty} e^{-i2\pi n f_o t_R} \left[\frac{\sin(n\pi f_o t_w)}{n\pi f_o t_w}\right]^2 \delta(f - nf_o) \qquad (4)$$

where $f_o = T_o^{-1}$ is the fundamental frequency and $\delta(x)$ the Dirac delta function. The cross-power spectrum is a complex quantity and, because of the periodicity of the cross-correlation function, consists of a series of discrete lines spaced at intervals $\Delta f = f_o$ on the frequency axis. For the case of several received pulses the analytical form of the cross-power spectrum, made up of the superposition of several such expressions as given in equation (4), becomes intractable.

As to the question of choice of function to serve as the ultrasonic signature, the cross-correlation function, in this specific application, shows an advantage over the cross-power spectrum in the facility of interpretation. A cross-correlation triangle, being directly associated with a particular received pulse, will reflect changes in the corresponding acoustical path. With regard to the cross-power spectrum, on the other hand, no such association is possible; furthermore, because the large pulses will dominate the spectrum, any changes attributable to the smaller pulses, which may bear crucial information, may not be noticeable. Once the reference cross-correlogram is recorded, then it is subtracted from succeeding cross-correlograms to yield the differential cross-correlogram, the quantity used as the signature. Not only does a differential measurement improve the sensitivity to small changes, but it also enables us to devote more of the computer memory to the changing instead of constant portions of the sample record.

The "coherence function," defined as

$$\gamma^2 = \frac{|G_{SR}|^2}{G_{SS}G_{RR}} \tag{5}$$

where G_{SS} and G_{RR} are the auto-power spectra of the transmitted and received pulses respectively, is a measure of the linear cause-effect relationship between $S(t)$ and $R(t)$. Although relatively insensitive to changes in the test specimens, the coherence function proves valuable in giving an indication of the quality of the bond between the transducers and the specimen. This will be discussed further in Section III-B.

III. INSTRUMENTATION AND DATA PROCESSING

A. The Electronic System

A block diagram of the electronic system is shown in figure 3. The tone burst generator 3 produces short bursts of the 5-6 MHz carrier voltage, which after amplification by the RF power amplifier 4 drives the transmitting transducer 16. The carrier frequency is locked to that of the reference oscillator 2 and monitored on the electronic counter 1. Ultrasonic pulses propagate through the specimen to the receiving transducer 13 and are amplified by the dual amplifier 7. Because it is required to feed only the pulse envelopes into the Fourier analyzer, the carrier is removed from the received and transmitted signals by means of mixers 8 and 9, respectively, for which the reference oscillator also serves as the local oscillator. The VHF attenuators 5 and 6 are used to control the amplitude of the signals from the reference oscillator and RF power amplifier. Preamplifiers 10 and 11 and logarithmic attenuator 12 condition the demodulated signals for viewing on oscilloscope 15, recording on magnetic tape recorder 14, and subsequent processing in the Fourier analyzer system.

The pertinent specifications and settings of the instruments used in the electronic system are shown in table I. For the most part the specifications are fixed, but those permitting adjustment are noted under "Remarks."

The settings of the tone burst generator are adjusted to accommodate other components of the system. A carrier frequency of 5.8-5.9 MHz, close to the series resonant frequency of the transducers, was found to yield the maximum output signal at the receiving transducer. A pulse width of

20 μsec, corresponding to about half the transit time across the plate, is sufficiently narrow to permit ample time for depicting events between multiple reflections. The pulse repetition period is not critical but must be longer than one record length (640 μsec) of the Fourier analyzer. The output amplitude is adjusted to utilize the maximum dynamic range of mixer 8, which demodulates the received pulse.

The VHF attenuators are adjusted for maximum linear mixer output.

The output of the mixers, which are of the double-balanced or "ring" modulator variety, are sensitive not only to the amplitude of the input and local oscillator signals but also to their phase difference. Because of the relatively long transit times of the received ultrasonic pulses, the phase shift at the receiver amounts to several hundred carrier cycles. Therefore slight changes in the carrier frequency cause considerable changes in the amplitude of the received pulses; as the carrier frequency increases, the pulse amplitudes become alternately positive and negative. The pulses received later in the period show greater phase sensitivity because of the greater delay in terms of number of carrier cycles. In order to minimize the phase sensitivity the carrier frequency was sometimes tuned to preserve the pattern of the latter two or three pulses of the sample period. The necessary adjustment in frequency between successive signatures was found to be typically no more than a few parts in 60,000. At other times the carrier frequency was held strictly constant, and the phase sensitivity was incorporated as part of the signature.

The bandwidth of the preamplifiers is adjusted wide enough to preserve the shape of the pulse envelopes but narrow enough to suppress low-

frequency noise and transducer ringing. The gain is adjusted for a 1.4 volt pulse height at the output in order to utilize the full dynamic range of the magnetic tape recorder.

The logarithmic attenuator consists of two parallel, but oppositely oriented, type 1N277 germanium diodes in series with a 10 kΩ resistor. The relationship between input and output is linear for output voltages below 100 millivolts and approximately logarithmic for output voltages above 1 volt. The function of this device is to enhance the role of the smaller pulses, which often bear information not contained in the larger pulses. As a result a greater share of the Fourier analyzer memory is devoted to the smaller pulses.

The use of a magnetic tape recorder to record the analog transducer signals was necessitated by the fact that the fatigue-testing machine and Fourier analyzer system were physically situated at different locations. After each interval of fatigue cycling it was not convenient to remove the specimen, transfer it to the site of the Fourier analyzer for a measurement, and then remount it in the fatigue-testing machine. Rather the entire electronic system was moved to the site of the fatigue-testing machine. Moreover the tape recording provides a permanent record of the analog transducer signals. For each signature the tape recorder was allowed to run for about 60 seconds, a time corresponding to 600 feet of tape and 30,000 analog records. The tape recorder reduces the bandwidth of the overall system from 100 to 80 kHz, but the quality of the signals showed no appreciable deterioration.

B. Specimens and Ultrasonic Transducers

All the experiments were performed on plates having dimensions 20 x 10 x 1/4 inch and made of aluminum alloy 6061, for which the applicable properties are listed in table II.

The properties of the Branson Z-101-CF lead metaniobate piezoelectric transducers used in the experiments are listed in table III. The capability of transducers made of this material to deliver high ultrasonic power at high frequency, despite a high dielectric permittivity, is attributable to a large piezoelectric stress constant. Lithium sulfate, a possible competitive material available commercially, is generally not used for solid-state testing because of a tendency to crack easily. The exceptionally high dielectric permittivity of the perovskites (barium titanate and the PZT series) leads to an extremely low shunt reactance, and quartz is handicapped by a relatively low piezoelectric stress constant and extremely narrow bandwidth.

The transducers were bonded to the test specimens with RTV-102 silicon rubber (General Electric Co.), which has the following desirable properties: (1) efficient acoustical coupling, (2) sufficient flexibility to withstand the large strains of fatigue loading, and (3) ease of application and removal. Following a rinse with methyl ethyl keytone, which was allowed to dry, the surfaces of both transducer and specimen were coated with the RTV-102. The transducer was pressed to the specimen surface and held in place under pressure with Scotch filament tape. The bond was allowed to set overnight. The tape was not removed during the subsequent testing. As mentioned in Section II, the coherence function offers a reliable indication of the quality of the bond. Figure 4 shows

the coherence function of a well-bonded transducer and that of a transducer with an intentionally impaired bond. During the testing of the specimens the coherence function was continually monitored, but not even under the severest fatigue cycling was an RTV-102 bond ever observed to fail.

According to Morse and Ingard (ref. 10) the intensity of radiation from a circular piston has the following angular distribution:

$$f(\theta) = \frac{\cos^2\theta}{|\beta + \cos\theta|^2}\left[\frac{2J_1(2\pi a\lambda^{-1}\sin\theta)}{(2\pi a\lambda^{-1}\sin\theta)}\right]^2 \qquad (6)$$

where $f(\theta)$ = angle-distribution factor, θ = angle measured from piston axis, a = diameter of piston, λ = wavelength of sound, and β is the ratio of the specific acoustical impedance of the medium to the radiation impedance of the transducer. Upon inserting the values $\lambda = 0.040$ inch, $a = 0.250$ inch, $\beta = 17/12.8 = 1.33$ (see tables II and III) into equation (6), we obtain the angular distribution of transmitted intensity shown in figure 5. From this we ascertain that the ultrasonic beam spreads about $\pm 5^{\circ}$ with respect to the transducer axis, its intensity falling off rapidly with angle. The distribution is subject to some uncertainty, however, because the effect of the transducer bond upon β is not taken into account.

C. The Fourier Analyzer System

The basic components of the Hewlett-Packard Model 5451A Fourier Analyzer System, in which the transducer signals were processed, are shown in figure 6. The analog data enters the system through the analog-to-digital (a-d) converter, where they are sampled at a selected rate;

the sample amplitudes are translated into bits of information and these are entered into the computer. Data already digitized may be entered through the tape reader, teletypewriter, or manually through the keyboard. The computer stores records of the sampled input data and processes the data according to a prescribed program. The keyboard is used to enter the program into the computer as well as any constants needed in the data processing. The contents of any of the data blocks (see below) can be monitored on the display oscilloscope, and can be recorded permanently in analog form on the x-y plotter or in digital form on the teleprinter (printout and/or punched tape). Complete specifications for the 5451A Fourier Analyzer System are available from the manufacturer.

The analog transmitting and receiving transducer signals were fed from the magnetic tape recorder into channels A and B, respectively, of the a-d converter. The sampling was triggered internally by the transmitted pulse on channel A. The sampling interval was chosen as the shortest possible in dual-channel operation, namely 5 μsec, which provided 4-5 samples per pulse. (The transmitted pulse was always 20 μsec wide, but the received pulses broadened as they propagated through the plate.) The input range selector was adjusted to accommodate the peak sample amplitude in the record.

The amplitude of a digitized data sample is represented by a 16-bit binary number, ranging from -32,768 to +32,768. This number, together with sign, is called a data word. The group of data words (i.e. samples) over one record constitutes a data block. The computer memory contains seven blocks: one processing block and six storage blocks. The block size - just the number of words (samples) per record - is always an

integral power of 2, ranging from 64 to 1024. For the current research a block size of 128 was chosen. The corresponding record length was 640 μsec (128 × 5 μsec), a time sufficiently long to include the essential part of the train of received pulses. A larger block size did not leave enough room in the 8K computer memory to complete the required processing. In order to reduce the effects of random inputs the cross-correlograms and other functions were averaged over 100 analog records. It was found by direct measurement that the corresponding processing time amounted to 47 seconds; thus the 60-second recording on magnetic tape provided ample time for 100 analog records to enter the Fourier analyzer. A summary of specifications pertaining to data processing is given in table IV.

A printout of the program used to compute the differential cross-correlograms is shown in teleprinter symbols in table V(a) and explained in table V(b). In table V(a) column 1 contains the program element number or step, as it will be called here, column 2 the command, column 3 a block number, and columns 4 and 5 either block numbers or constants. Because the 8K computer memory contains only 100 program element locations, the program is interrupted at step 74 for several manual operations. Upon completion of the program operations the computer memory contains the following:

Block	0	differential cross-correlogram (used as the signature)
	1	sampled record of transmitted signal
	2	sampled record of received signal
	3	normalizing factor (see note 2, table V(b))
	4	normalized cross-correlation function (see note 3, table V(b))
	5	differential cross-power spectrum
	6	reference cross-correlogram.

The contents of block 0 were recorded on the x-y plotter and the contents of block 4 were printed and punched. A second program was used to compute the auto-power spectrum of the received signal, the transfer function, and the coherence function. Complete details concerning the programing of the Fourier analyzer may be found in reference 11.

The program of table V(a) points out one of two distinct useful features of the Fourier analyzer system - the capability of rapid processing immediately after accepting an analog record, as evidenced by the data-editing operation of step 17 and the normalizing operation of steps 22-30. The utility of the second feature - the capability of processing selected portions of a block - will become evident in succeeding sections of this report.

Closely related to the time domain parameters - sample interval Δt, record length T, and block size N - are the frequency domain parameters - frequency resolution Δf and maximum frequency F_{max} of an analyzer spectrum (ref. 12):

$$F_{max} = 1/2\ \Delta t \tag{7}$$

$$\Delta f = \frac{1}{T}. \tag{8}$$

Using the values $\Delta t = 5$ μsec and $T = 640$ μsec given in table IV, we find $F_{max} = 100$ kHz and $\Delta f = 1565$ Hz. In order to avoid aliasing (ref. 13) it is necessary that

$$F_{max} > f_{max} \tag{9}$$

where f_{max} is the maximum frequency in the analog record. Because the upper frequency of the electronic system is 80 kHz, the inequality (9) is satisfied.

IV. SOME ACOUSTICAL CONSIDERATIONS

The geometrical arrangement of the transducers on the plate, as used in most of the experiments, is shown in figure 7. Because of the continuous angular distribution of the transmitted ultrasound, pulses may reach the receiver over several possible paths. Let us call each one-way trip across the plate a pass; let the integer n designate the number of passes a pulse makes in going from the transmitter to the receiver. Pulses may reach the receiver by way of the direct path ($n = 1$) or a secondary path ($n > 1$), the latter involving reflections from exterior boundaries. These pulses constitute the principal sequence (to borrow a term from spectroscopy). It is evident from symmetry that such pulses must travel through the center C and must make an odd number of passes across the plate ($n = 1, 3, 5, \ldots$) in order to reach the receiver.

Figure 8(a) shows the principal sequence or train of pulses prior to the introduction of a defect into the plate. The vertical amplifier of the oscilloscope is set in the "add" mode to permit the transmitted and received pulses to appear on one sweep. Thus the transmitted pulse appears at the beginning of the sweep, the direct pulse arrives at the receiver approximately 43 μsec later, and the secondary pulses arrive approximately at odd integral multiples of 43 μsec. The amplitudes of the received pulses are on an approximately logarithmic scale. The frequency is tuned to make the first five received pulses positive, but an attempt to make the sixth positive results in distortion of the earlier pulses.

The particular angles θ_n (radiation angles) for which pulses suceed in arriving at the receiver are determined simply by the law of reflection, from which the following result is derived (see fig. 7):

$$\tan \theta_n = L_1/nL_2. \tag{10}$$

The values of θ_n for the first several values of n are listed in table VI. As the radiation angle θ_n increases the radiated intensity decreases; but at the same time the number of passes n, the path length, and the attenuation decrease. The first effect favors pulses radiated at small θ_n, but the second effect favors those radiated at large θ_n. Therefore we expect the received pulse height to reach a maximum somewhere between the two ends of the received pulse train - a conclusion borne out by figure 8(a). The large angle of the direct pulse indicates that it is radiated from a side lobe (see fig. 5). The error in angle due to the uncertainty in β, mentioned in Section III-B, probably allows the three-pass pulse to be included in the main lobe, as its large amplitude in figure 8(a) strongly suggests.

It has been determined experimentally that the pulse amplitude decreases at a rate of about 0.8 dB/inch. Theoretical consideration of the beamwidth indicates that the loss is almost entirely due to spreading.

As a consequence of the close spacing of the radiation angles θ_n and of the 1/4 inch beamwidth of the pulses leaving the transmitter, the sequence of principal pulses sweeps over and thus monitors the entire area between the transducers, except for a small region on the vertical centerline near each edge of the plate.

V. EXPERIMENTS ON A SIMPLE SPECIMEN WITH A SIMULATED DEFECT

A. Experimental Procedure

This experiment was designed to test the sensitivity of the system to a small defect introduced into the specimen. After a reference cross-correlogram was recorded, signatures were taken after introduction of the defect and after successive increases in its size.

The locations of the defect, a small drilled hole, and the transducers are shown in figure 9. The drill size was initially number 80 (13.5 mil = 0.0135 inch diameter) and was increased each time by five drill sizes up to number 5 (205.5 mil diameter). The hole was located on the vertical centerline of the plate, but off center, so that blockage of the principal pulses passing through the center was minimal. A pulse passing through the site of the hole would not ordinarily have reached the receiver. However, the presence of the hole, a scattering center, caused a portion of the incident pulse to divert toward the receiver. After each increase in hole diameter it was found that the carrier frequency had to be retuned slightly in order to maintain a consistent pulse pattern, as explained in Section III-A.

B. Experimental Results

Figures 8(a) to 8(q) show the transmitted pulse and the train of received pulses of plate 10 for each hole diameter. The corresponding differential cross-correlograms are shown in figures 10(b) to 10(q). The reference cross-correlogram (no hole) in figure 10(a) shows the cross-correlation triangles for the first six principal pulses, labelled P_1, P_3, . . ., P_{11}, where the subscript designates the number of passes

across the plate. The differential cross-correlograms are for the most part much smaller than the reference, as is evidenced by the one-to-ten ratio of scale factors.

In the vicinity of the principal pulses the differential cross-correlograms are fairly constant, showing little or no change as the hole size increases. (Pulse P_{11} is an exception and will be discussed later.) The interesting changes are found in the regions between the principal pulses. For example, the region midway between P_1 and P_3 is strongly negative for hole diameters of 70, 110, 149.5, and 205.5 mils, and near zero or slightly positive for hole diameters of 35, 98, 128.5 and 180 mils. Even more prominent are the fluctuations in the region between pulses P_3 and P_5. If we attribute this activity to the appearance of small pulses scattered from the hole, then the pulse between P_1 and P_3 has a transit time of 75 μsec, corresponding to approximately two passes across the plate; that between P_3 and P_5 has a transit time near 175 μsec, corresponding to approximately four passes across the plate.

The pulses between the principal pulses we designate as <u>satellite pulses</u> with the symbol Q_n, where the subscript indicates the equivalent number of passes across the plate. The manner in which the satellite pulses reach the receiver after scattering is illustrated in figures 11(a) to 11(d). A satellite pulse corresponding to a given number of passes may reach the receiver over more than one acoustical path. If the incident wave approaches the hole from above, the satellite pulse is marked with a prime; if from below, it is marked with a double-prime. The primed pulses reach the receiver slightly earlier than the double-primed pulses because the hole is situated somewhat above the center of the

plate. Thus each satellite pulse appears as a doublet. Because of a large radiation angle pulse Q_2'' has a much lower amplitude than the other satellite pulses and will be neglected. The locations where we expect to find pulses Q_2', Q_4', and Q_4'' are indicated by the cross-correlation triangles of figure 10(r).

The amplitude fluctuations of the satellite pulses with increasing hole size are a manifestation of wave reinforcement and interference and will be treated in detail in Section V-C. In order to investigate the dependence of pulse height upon hole diameter, we use the Fourier analyzer to integrate the differential cross-correlogram over the intervals associated with the cross-correlation triangles Q_2', Q_4', and Q_4'', and then to divide by the time base. In the latter two cases the integration is carried out to or from the point of intersection. The average values obtained by this procedure are taken to be representative of the satellite pulse heights,[2] which are plotted versus hole diameter in figure 12. The plot clearly reveals the presence of the hole at a diameter equal to a wavelength of ultrasound, or a little less, and provides an emphatic indication of its subsequent growth.

As mentioned previously, the principal pulses, in passing through the center of the plate, avoid the hole and are immune to the effects of increasing hole diameter until the hole grows large enough to block out a portion of the beamwidth. The earliest principal pulse to suffer blockage will be the one approaching the center at the smallest angle, i.e., the pulse making the greatest number of passes across the plate. In our case

---

[2]The same averaging procedure will be used in the later experiments.

this is P_{11}, the last pulse included in the analog record. A plot of the average differential pulse height P_{11} (see above) versus hole diameter is shown in figure 13. Despite the variance in the data the differential cross-correlation between P_{11} and the transmitted pulse yields a quite consistent increase with increasing hole size.

C. Analysis of Results

The solution to the problem of the scattering of a plane acoustic wave from a rigid cylinder in a fluid is ready available in texts on acoustics (ref. 14). K. P. Moy has considered the scattering of a plane acoustic wave from a circular hole in an elastic medium - a closely related problem pertinent to the current research (ref. 15). There are two fundamental differences between the two problems:

(1) The radial velocity of the fluid vanishes at the boundary of the cylinder, but the acoustical pressure vanishes at the boundary of the hole.

(2) The shear rigidity is zero for a (lossless) fluid but generally nonzero for an elastic medium, where we thus expect mode conversion to take place. This is considered negligible in Moy's analysis.

In the configuration of plate 10 the distance between the point of observation (the receiver) and the scattering center (the hole) is not extremely large compared to the size of the scattering center but is much larger than the wavelength of the ultrasound. Under these conditions the receiver lies within the Fresnel zone, where subtle interaction between the incident and scattered waves occurs. The far-field, short-wavelength ($\lambda \ll 2\pi r_o$) expressions for the acoustical intensity and pressure are found by Moy to be the following:

$$I = \frac{I_o r_o}{2r}\left[\sin\left(\frac{\phi}{2}\right) + \frac{1}{\pi k r_o}\cot^2\left(\frac{\phi}{2}\right)\sin^2(kr_o\phi)\right] \tag{11}$$

$$p = p_o\sqrt{\frac{2}{i\pi kr}}\, e^{-ikr_o} \sin k(r - r_o)\, \frac{\sin\left[\left(kr_o + \frac{1}{2}\right)(\phi - \pi)\right]}{\sin\frac{1}{2}(\phi - \pi)} \tag{12}$$

where I_o, p_o = incident intensity and pressure

I, p = far-field intensity and pressure

r = distance from center of hole

r_o = radius of hole

ϕ = scattering angle referred to direction of incident wave

$k = 2\pi/\lambda$ = wave number of ultrasound.

The scattering pattern of the intensity is plotted in figure 14 for the case $r_o = 2.57\lambda$, corresponding to the largest hole drilled into the plate. The forward scatter, producing the "shadow-forming" wave, is large but highly directional. There are two prominent side lobes close to $\phi = \pm 18^o$, but the remainder of the scattering is reasonably uniform about the periphery of the hole. A receiver can thus detect a scattered signal at any angle relative to the direction of the incident wave.

To calculate the pressure of the scattered wave at the receiver, we must take into account the sensitivity of the receiver electronics to the phase difference between the transmitted and scattered waves. We lump the inherent phase shift with that due to retardation of the scattered wave into a single phase angle ϕ_o and rewrite equation (12) as follows:

$$p = K \sin(\phi_o - kr_o)\, \frac{\sin\left[\left(kr_o + \frac{1}{2}\right)(\phi - \pi)\right]}{\sin\frac{1}{2}(\phi - \pi)} \,. \tag{13}$$

The average pressure p_R at the receiver is

$$p_R = \frac{K \sin(\phi_o - kr_o)}{2\phi_1} \int_{\phi_R-\phi_1}^{\phi_R+\phi_1} \frac{\sin\left[\left(kr_o + \frac{1}{2}\right)(\phi - \pi)\right]}{\sin\frac{1}{2}(\phi - \pi)} d\phi \qquad (14)$$

where ϕ_R = angle of scatter toward the receiver (see fig. 11(a))

$2\phi_1$ = angle subtended by the receiving transducer.

We note that in the integrand the argument of the numerator varies much more rapidly with ϕ than that of the denominator, which remains nearly constant over the interval of integration. Upon setting $\phi = \phi_R$ in the denominator, carrying out the elementary integration, and employing some trigonometric identities we find

$$p_R = K \sin(\phi_o - kr_o) \frac{\sin\left[\left(kr_o + \frac{1}{2}\right)(\phi_R - \pi)\right]}{\sin\frac{1}{2}(\phi_R - \pi)} \frac{\sin\left(kr_o + \frac{1}{2}\right)\phi_1}{\left(kr_o + \frac{1}{2}\right)\phi_1}. \qquad (15)$$

The quantities ϕ_1 and ϕ_R are determined by simple geometrical considerations, and ϕ_o and K are fitted to the data. A plot of equation (15) with the parameter values given in the caption, along with the experimental values of p_R evaluated from the differential cross-correlograms, is shown in figure 15 for $2r_o > 100$ mils. As may be seen from figure 12, the pulse height of Q_2' fluctuates about some average value; this is subtracted off in fitting the data to the theoretical expression, equation (15). Below $2r_o = 100$ mils the short-wavelength approximation fails and the fit becomes progressively worse with decreasing hole diameter.

Although the experimental data points do not show a really good fit to the theoretical curve - a difficult accomplishment in acoustical Fresnel scattering - they do present the basic features of the dependence of the scattering upon hole diameter. We conclude that ultrasonic signature analysis, as described here, has successfully led to the extraction of meaningful scattering data from the barely discernible fluctuations of Q_2' in figures 8(a) to 8(q).

VI. EXPERIMENTS ON A SIMPLE SPECIMEN WITH FATIGUE-INDUCED DEFECTS

A. Experimental Procedure

The purpose of the series of experiments described in this section was to determine the sensitivity of the ultrasonic signature to the initiation and subsequent growth of cracks in specimens subjected to fatigue cycling.

In order to expedite the nucleation of the crack, a slot AB, 0.015 inch wide by 1 inch long as shown in figures 16(a)-(c), was spark-machined into the specimen by the "Elox" process. The figures also show the six holes for gripping the specimen in the machine, a Carl Schenck Fatigue-Testing Push-Pull Machine Model No. PB 10/60, as well as three different arrangements of the transducers. The stress was applied normal to the slot, and the cracks, starting at edges A and B, grew outward and parallel to the slot.

After a specimen was mounted into the machine, a measurement was made that would later provide the reference cross-correlogram. Then the mean and alternating loads were applied. After a specified interval of fatigue cycling the crack length was measured (if the crack had appeared),

the machine stopped, and the mean load removed for another ultrasonic measurement.

The number of cycles required to initiate a crack was found to depend critically upon the load. Under a mean load of 3.5 kpis and an alternating load of $\pm$3.5 kpis - values applying to all but one of the specimens - the crack was first observed between 30,000 and 100,000 cycles (in most cases shortly after the lower figure). The lone exception was plate 3, to which a load of 3.75 $\pm$ 3.75 kpis was applied. For this specimen a crack was observed shortly after 7000 cycles. The cycling frequency ranged from 1030-1130 cycles per minute, depending upon the specimen and the load.

In the course of the fatigue cycling the edges of the slot A and B were continuously observed under a microscope. Illumination of these regions by a stroboscope at a frequency slightly different from the fatigue-cycling frequency enhanced the distinguishability of the crack, in that its opening and closing under the alternating stress could be observed. Finding a crack and measuring its length in the early stages of growth was difficult. Although 10-mil cracks were observable, meaningful quantitative measurements using the microscope reticle could not be carried out until the crack length reached at least 20 mils. A greater length was easier to measure despite the difficulty in finding the tip of the crack.

The fatigue loading of a specimen was interrupted for an ultrasonic measurement on the following occasions:

(1) At selected intervals before the appearance of the crack, in order that the precrack history of the specimen be monitored and the reference conditions established

(2) Immediately after a crack was first observed, in order to determine the immediate effect of the crack upon the ultrasonic signature

(3) At specified lengths during subsequent crack growth, in order to relate increases in crack length to changes in the signature.

For plates 3 and 4 the carrier frequency was retuned prior to each ultrasonic measurement; but for plates 5, 6, and 7 this practice was stopped, and all the signatures of a plate were obtained at the same frequency. Once mounted into the fatigue-testing machine, a plate was never removed until its entire test program was completed.

B. Experimental Results for Plates 3 and 6

The arrangement of the transducers is shown in figure 16(a). The ultrasonic pulse trains of plate 6 after selected intervals of fatigue cycling are shown in figure 17. The pulse train of figure 17(a) corresponds to the prefatigued condition of the plate. We note two sequences of pulses: the principal pulses, having transit times of approximately 43, 129, 215, and 301 μsec, and, in addition, satellite pulses having transit times of approximately 80, 160, and 240 μsec. Because the latter times correspond to even numbers of passes across the plate, the satellite pulses are interpreted as reflections from edge A of the slot back toward the receiver. After 30,200 fatigue cycles the satellite pulses disappear altogether (see figs. 17(b) and (c)). The disappearance of the satellite pulses manifests itself by the appearance of new cross-correlation triangles Q_2, Q_4, and Q_6 in the differential cross-correlograms of figure 18. Using the averaging procedure described in Section V-B, we

show the satellite pulse heights against the number of fatigue cycles in figure 19. The results for plate 3 are similar.

The crack was first observed under the microscope at 33,600 fatigue cycles. The machine had been stopped at 30,200 cycles in accordance with our intention to obtain a precrack signature. However, the plots of figure 19 clearly indicate the appearance of the crack some time before its detection under the microscope. Unfortunately the machine had not been stopped early enough for a comparison of the precrack differential satellite pulse heights with those shown in figure 19.

Under the conditions of this experiment the satellite pulses were large enough that the cross-correlation technique did not offer much advantage. However this will generally not be the case for a complex structure, where we might expect the technique to play an essential role in the detection of cracks that go unnoticed by direct inspection.

C. Experimental Results for Plates 4 and 7

The transducer arrangement and resulting ultrasonic pulse trains of plate 7 are shown in figures 16(b) and 20. The principal pulses P_1, P_3, P_5, P_7, P_9, and P_{11} appear at approximately 45, 130, 215, 300, 385, and 470 μsec, respectively, and a prominent satellite pulse Q_4 at 175 μsec, interpreted as a reflection from either edge A or B. The possible acoustical paths over which Q_4 may be realized are analogous to those shown in figures 11(c) and (d). Evidently the stronger reflections of Q_2, Q_6, etc. occur at such angles as to miss the receiver R. The differential cross-correlograms of plate 7 are shown in figure 21; those of plate 4 are similar. In figures 22-25 are plotted the average

pulse heights versus the number of fatigue cycles for the principal and satellite pulses of both plates.

Three different physical mechanisms are operative by which the crack causes changes in the signature:

(1) The appearance of the crack causes the immediate disappearance of satellite pulse Q_4, as indicated by the rapid increase in differential pulse height shown in figures 23 and 25. This effect is most dramatic in plate 4, where the differential pulse height of Q_4 jumps over eightfold upon the appearance of the crack.

(2) As the crack grows longer and wider, it will tend to block those principal pulses incident upon the slot at the larger angles (first P_1, then P_3, and so on). The concomitant growth of the crack and pulse P_1, evident in figures 22-24, is believed attributable to this mechanism.

(3) The received pulses suffer slight shifts in phase as fatigue progresses. Because the output of the electronic system is sensitive to the phase difference between the transmitted and received pulses, the phase shifts will show up as changes in the received pulse height. Although all the principal pulses will be affected to some degree, the effect will be more pronounced for those pulses travelling over the longer acoustical paths - a conclusion supported by the rapid growth of principal pulse P_9 in figures 22 and 24.

It is interesting to note from the comparative growth of P_1 and P_9 that mechanism 2 is dominant in plate 4, but mechanism 3 is dominant in plate 7, as far as the principal pulses are concerned. The retuning of the carrier frequency evidently reduced the effect of the phase shift of the principal pulses in plate 4.

D. Experimental Results for Plate 5

An indentation was machined on each side of plate 5, as shown in figure 16(c), in order that the blockage of the direct pulses by the crack could be studied. The indentations lay at such an angle that the transmitted beamwidth had six mils clearance on each side of the slot. Figure 26 clearly shows the growth of the differential pulse height of P_1 and P_3 as fatigue progresses, indicating increasing blockage of the principal pulses. It is apparent that the blockage becomes effective only long after the crack is first observed and its length exceeds the wavelength of ultrasound (λ = 40 mils).

VII. EXPERIMENTS ON A RIVETED SPECIMEN

In this experiment the sensitivity of the system to a crack developing under a rivet head - a location inaccessible to visual inspection - was tested. Holes were drilled into a plate at locations A, B, and C in figure 27 in order to accommodate three aluminum rivets (type AN 442-2117-T3, 3/8 inch dia. x 1-7/16 inch long). Because no crack nucleation center was machined into the plate, the latter was necked from a width of 10 to 8-1/2 inches to increase the stress in the vicinity of the rivets. Two receiving transducers were mounted on opposite edges of the plate in an attempt to gather information concerning each of the three rivets individually. Transducer R_1 receives the "odd" principal pulses P_1, P_3, P_5, . . ., all of which pass through the center rivet B. Transducer R_2 receives the "even" principal pulses, of which P_2, P_6, P_{10}, . . . pass near or partly through the upper rivet A, and P_4, P_8, P_{12}, . . . near or partly through the lower rivet C. The paths of a few of these pulses are shown in figure 27.

Although the test procedure was similar to that of the slotted plates, the presence of the rivets produced two major changes in the experimental conditions. The rivets, made of the same material as the plate and pressed into compression, caused the plate to appear homogeneous both acoustically and mechanically; as a result the ultrasonic pulses were relatively insensitive to the plate-rivet boundary. Secondly, the stress was not intensified around the holes and had to be raised to excessively high levels in order to effect a change in the signature. Because of the difficulty in estimating the stress levels needed to initiate a crack within a reasonable number of cycles, the load was gradually increased until changes in the signature became apparent. The plate was cycled according to the following load schedule, and a significant change in the signature did not occur until the final load was applied:

(1)	130,000	cycles @	5	± 5 kpsi	
(2)	99,900		7.5	± 7.5	
(3)	48,200		10	± 10	(exceeds yield stress)
(4)	141,300		12.5	± 12.5	
(5)	172,500		20	± 10	
(6)	62,800		20	± 15	(exceeds ultimate stress).

In the course of the final loading the ultrasonic measurements were taken at 30,000 and 62,800 cycles, at which time a severe vertical crack, running through the location of rivet C, caused the fatigue-testing machine to stop. The rivets were removed and the periphery of the holes examined. All the holes were found elongated in the direction of the stress, but no cracks were found around holes A and B.

The differential cross-correlograms of the signals at R_1 and R_2 are shown in figure 28. Because only two signatures were taken, the differential pulse heights are not plotted against the number of cycles, as previously, but are compared at 62,800 and 30,000 cycles in the manner shown in figure 29. The increase in pulse height with increasing number of cycles is interpreted as blockage of the principal pulses due to elongation of the holes. Pulses P_4 and P_8, passing near or partly through rivet C - the site of the crack, show no more sensitivity to the number of fatigue cycles than, say, P_2 or P_3, neither of which had passed near the crack. Thus, in this experiment, it is not possible to assess the effect of the crack upon the signature. To do so would require further investigation, whereby the stress level is made large enough to produce a crack eventually without elongating the hole. An alternate possibility is discussed in the Conclusions, Section VIII.

VIII. CONCLUSIONS

A. Achievement of Goals

The results of the experiments performed under this research clearly establish that the goals of phases 1 and 2 have been achieved. The ultrasonic signature has proved responsive to several of the physical mechanisms listed in the Introduction, and the instrumentation has proved sufficiently sensitive to detect small changes in the specimens that would have otherwise gone unnoticed. The experiments on plate 10 have demonstrated our ability to detect a small hole in an unspecified location in a plate. The remarkable sensitivity of the signature to the effects of diffraction and scattering are borne out in figures 12 and 13. On

plates 4-7 we have used the signature to detect fatigue cracks during the early stages of growth. Here we have observed the effects of diffraction (figs. 22, 24, and 26), reflections from interior boundaries before and after modification by the cracks (figs. 19, 23, and 25), and shifts in phase between transmitted and received pulses (P_9 in figs. 22 and 24). The signature of plate 6 (fig. 19) had even revealed the presence of the crack prior to observation under the microscope. In plate 8, the riveted specimen, we have seen evidence of scattering from an elongated hole, but detection of a crack under a rivet head has not been truly tested.

The change in absorption of ultrasound following the appearance of the crack proved too small to have a marked effect upon the signature. Most of the principal pulses, in passing over the crack, showed but little change in pulse height, as may be seen in figure 22. As for the other possible mechanisms mentioned in the Introduction, the limited bandwidth of the instrumentation eliminated the contribution of harmonic generation, and the absence of shear transducers precluded investigation into mode conversion.

B. Advantages of the Method

The method described here incorporates three features to improve the signal-to-noise ratio not normally found in a conventional pulse-echo measurement:

(1) A logarithmic attenuator in the receiving electronics to enhance the significance of the small satellite pulses, which ofttimes bear information not contained in the principal pulses

(2) Cross-correlation between the transmitted and received pulses as a means of eliminating random and incoherent signals

(3) Differential data analysis, whereby cross-correlation triangles are subtracted from reference triangles. This feature makes more room in the computer memory for the changing instead of constant portions of the sample record.

Several additional advantages have come to light in the course of the experimentation. The transducers can be arranged so that the ultrasound sweeps over wide regions of the specimen. The location of the hole in plate 10 (fig. 9), for example, is actually unfavorable as far as its effect upon the signature is concerned. A location removed from the vertical centerline would be preferred, for the hole would then block one or more principal pulses and have a more pronounced effect. In addition, the use of the coherence function to monitor the quality of the transducer bond, especially in cases where the bond is located in an area subjected to severe loading, is a decided advantage. Finally the Fourier analyzer system is capable of performing on-line data editing and processing according to a prescribed program. We have availed ourselves of this capability, for example, in deleting the pickup at the beginning of the received pulse train, in normalizing the transmitted pulse, and in computing average pulse heights over specified intervals of the analog record.

C. Possible Improvements

The most significant need for improvement lies in the reproducibility of a consistent received pulse train. It was often difficult to determine whether changes in the received pulse train were attributable to bona fide fatigue or to a need for retuning. The latter may have arisen from changes in the transducers or changes in the specimen not related to fatigue (e.g. rise in temperature). The rather sizeable fluctuations in

the growth of pulse P_{11} in plate 10 with increasing hole diameter (see fig. 13) followed from the uncertainty in the proper carrier frequency. The question of whether or not to hold the carrier frequency strictly constant, as was done for plates 5-7, in order to obtain the truest representation of the signature warrants further investigation.

An additional improvement in the sensitivity may be realized by sweeping the carrier frequency from a minimim to a maximum value over the duration of the pulse - a technique used in radar ranging. In this case the carrier of the received pulse will differ from that of the transmitted pulse not in phase but in frequency. If the sweep is accurately linear, then the demodulated received signal will have a frequency equal to the difference between the transmitted and received carrier frequencies. The cross-power spectrum will then be especially sensitive to small changes in transit time of the received pulses.

The experiment to determine the sensitivity of the signature to cracks developing under the head of a rivet should be repeated with two or more plates riveted together. If the ends of two different plates are bolted into the grips of the fatigue-testing machine, then the stress will be transmitted across the rivets and the signature will yield information concerning conditions in the vicinity of the rivets.

D. Status of the Ultrasonic Signature Analysis Program

The results of the research described herein may be briefly summarized as follows:

(1) The developmental work on the instrumentation used in ultrasonic signature analysis has been successfully completed. Existing instrumentation can be used to continue the program into the analysis of signatures of complex structures.

(2) The practicability of ultrasonic signature analysis has been demonstrated in view of the encouraging results attained on simple plates. The signatures obtained in the experiments described above lend themselves to simple interpretation, but this will generally not be the case for a complex structure, where, it is anticipated, prominent changes in the signature can be related to mechanical deterioration of the structure only through experience.

In accordance with these considerations we conclude that the ultrasonic signature analysis program is ready to proceed into phases 3 and 4.

ACKNOWLEDGMENTS

The principal investigator gratefully acknowledges the assistance rendered by the following personnel of Langley Research Center: A. M. Rackley, Instrument Research Division, for assistance in preparing the specimens; M. C. Hudson, Materials Division, and F. S. Moore, Jr., Operations Support Division, for assistance in setting up the fatigue-testing program; H. L. Freeman, Jr., Operations Support Division, for assistance in operating the fatigue-testing machine; and Mrs. Mary L. Edwards for typing the manuscript.

Special thanks are due Dr. S. L. Seaton, Chairman of the Ad Hoc Committee on Fatigue Detection, and Harlan K. Holmes, committee member, for suggesting ultrasonic signature analysis as a potential means of fatigue detection in complex structures.

REFERENCES

1. A. Z. Kiss, Hewlett-Packard Journal, June 1970.

2. R. Truell, C. Elbaum, and B. B. Chick, Ultrasonic Methods in Solid State Physics, Academic Press, New York (1969), pp. 41-52.

3. A. Granato and K. Luecke, J. Appl. Phys. 27, 583 (1956).

4. R. C. McMaster, Nondestructive Testing Handbook, vol II, Roland Press, New York (1963), p. 43-17.

5. J. S. Bendat and A. G. Piersol, Measurement and Analysis of Random Data, Wiley, New York (1966).

6. Y. W. Lee, Statistical Theory of Communication, Wiley, New York (1960).

7. K. P. Moy, Master's Thesis, Youngstown State University (1973).

8. See reference 5, p. 30.

9. See reference 7, p. 9.

10. P. M. Morse and K. U. Ingard, Theoretical Acoustics, McGraw-Hill, New York (1968), p. 381.

11. Fourier Analyzer System 5451A Operating Manual, Hewlett-Packard Company, Santa Clara, California (1972).

12. Application Note 140-0, "Fourier Analyzer Training Manual," Hewlett-Packard Company, p. 2-5.

13. See reference 12, p. 3-3.

14. See reference 10, pp. 400-404.

15. See reference 7, pp. 12-21.

TABLE I.- SPECIFICATIONS AND SETTINGS OF ELECTRONIC INSTRUMENTATION

	Instrument	Specifications and settings		Remarks
3.	Tone burst generator	Carrier frequency	5.8-5.9 MHz	All except synchronous range adjusted.
		Pulse width	20 μsec	
		Pulse repetition period	2000-4000 msec	
		Pulse height	1 V	
		Synchronous range	Within 1% of ref. osc. frequency	

	Instrument	Bandwidth	Gain	Remarks
4.	RF power amp	0.120-120 MHz	50 dB	50Ω output impedance, 50W max output power.
5.	VHF attenuator	dc-1000 MHz	-20 dB	Attenuation adjusted.
6.	VHF attenuator	dc-1000 MHz	-52 dB	Attenuation adjusted.
7.	Dual amplifier	0.1-400 MHz	40 dB	
8.	Mixer	0.2-500 MHz	-	
9.	Mixer	0.2-500 MHz	-	
10.	Preamplifier	$3-10^5$ Hz	20-54 dB	Gain and BW adjusted.
11.	Preamplifier	$3-10^5$ Hz	20 dB	Gain and BW adjusted.
12.	Log attenuator	dc-1 MHz	-	Logarithmic for outputs >1V.

	Instrument	Specifications	
14.	Magnetic tape recorder	Recording mode	FM, double extended response
		Band	Wideband group 1
		Bandwidth	dc-80 kHz
		Tape speed	120 ips
		Tape size	1 inch wide x 7200 feet long, wound on 14-inch reel

TABLE II.- PROPERTIES OF ALUMINUM ALLOY 6061

Property	Units	Value	Reference
Density	kg/m^3	2700	a
Young's modulus	N/m^2	7.1×10^{10}	a
Yield stress	kpsi	18	b
Ultimate stress	kpsi	32	b
Sound velocity (compressional waves)	m/sec	5920	c
Acoustic impedance	kg/m^2 sec	17×10^6	a

References

a. L. E. Kinsler and A. R. Frey, Fundamentals of Acoustics, 2 ed., Wiley, New York (1962).

b. Material Properties Handbook, vol. I, Advisory Group for Aerospace Research and Development (1958).

c. Own measurement.

TABLE III.- PROPERTIES OF THE ULTRASONIC TRANSDUCERS

Material: lead metaniobate

Type of wave: compressional

Property	Units	Value	Reference
Piezoelectric stress constant e_{33}	c/m^2	1.97	a
Elastic stiffness c_{33}	N/m^2	27×10^9	a
Dielectric permittivity ϵ_{33}		180	a
Sound velocity	m/sec	2130	b
Acoustic impedance	J sec/m^4	12.8×10^6	b
Mechanical quality factor		11	a
Transducer diameter	inch	0.250	
Series resonant frequency	MHz	8.5	c
Parallel resonant frequency	MHz	27	c
Shunt capacitance	pf	92.4	c
Series capacitance	pf	837.7	c
Series inductance	μH	0.421	c
Series resistance	Ω	3.7	c

References

a. O. F. Mattiat, Ultrasonic Transducer Materials, Plenum Press, New York (1971).

b. Computed from material data.

c. Own measurement. Values are for the transmitting transducer.

TABLE IV.- SPECIFICATIONS PERTAINING TO DATA PROCESSING

Magnetic Tape Recorder	
Recording time per signature	60 sec
Pulse repetition interval (duration of analog record)	2000 μsec
Number of analog records per signature	30,000
Fourier Analyzer System	
Block size N (number of samples per record)	128
Sample interval Δt	5 μsec
Record length T	640 μsec
Number of records averaged	100
Processing time per signature	47 sec

TABLE V(a).- PROGRAM USED TO COMPUTE DIFFERENTIAL CROSS-CORRELOGRAMS

Column 1	Column 2	Column 3	Column 4	Column 5
1	L	Ø		
4	CL	3		
7	CL	4		
1Ø	L	1		
13	RA	1	1	
17	CL	2	Ø	6
22	X<	1		
25	*			
27	A+	3		
3Ø	X>	3		
33	F	1	2	
37	X<	2		
4Ø	*-	1		
43	A+	4		
46	X>	4		
49	#	1	1ØØ	Ø
54	:	3	1ØØ	
58	:	4	1ØØ	
62	F	4		
65	$	3	Ø	6
7Ø	W	3	6	
74	J	3		
77	L	2		
8Ø	X<	4		
83	A-	6		
86	X>	5		
89	F	5		
92	L	3		
95	.			

TABLE V(b).- EXPLANATION OF PROGRAM TO COMPUTE DIFFERENTIAL CROSS-CORRELOGRAMS

Step	Operation
1-7	Accumulator Blocks 3 and 4 cleared.
13	128 samples of data accepted from a-d converter: transmitted signal into Block 1, received signal into Block 2.
17	First seven words (0-6) of Block 2 cleared (see note 1).
22-30	Transmitted pulse squared and result accumulated in Block 3 (see note 2).
33-46	Cross-power spectrum computed and accumulated in Block 4.
49	Computer instructed to repeat steps 33-46 until sequence is executed for 100 records.
54-58	Contents of Blocks 3 and 4 divided by 100 to obtain mean values.
62	Fourier transform of Block 4 computed to obtain cross-correlation function.
65-74	Block 3 integrated to obtain normalizing factor, which is printed out. Program jumps to step 92 and then computer stops.
Manual	See note 3.
77-86	Differential cross-correlogram computed and stored in Block 0.
89-91	Differential cross-power spectrum computed and stored in Block 5.
95	Computer stops.

Notes

1. Despite careful grounding and shielding the transmitted pulse was found to radiate directly into the receiving electronics and produced a small, extraneous pulse in the sequence of received pulses. This pulse is removed by clearing words 0-6, corresponding to the first 30 μsec of the received signal, of Block 2.

2. This will be used later (steps 65-74) in the computation of the normalizing factor $I = \int \left[S(t)\right]^2 dt$ in order to account for possible changes in the transmitted pulse from signature to signature.

3. The manual operations are as follows:

   For the base signature the cross-correlogram is stored in Block 6, where it remains as the reference cross-correlogram. The contents of Block 6 are typed on the teletypewriter and punched on tape. Program continued at step 77.

   For successive signatures the cross-correlogram in Block 4 is multiplied by the base normalizing factor and divided by the normalizing factor of the current signature, both factors entered through the keyboard. Program continued at step 77.

TABLE VI.- RADIATION ANGLE θ_n VERSUS NUMBER OF PASSES n ACROSS THE PLATE

L_1 = 3 inches

L_2 = 10 inches

n	θ_n
1	16.7°
3	5.71°
5	3.43°
7	2.45°
9	1.91°
11	1.56°
13	1.32°
15	1.15°

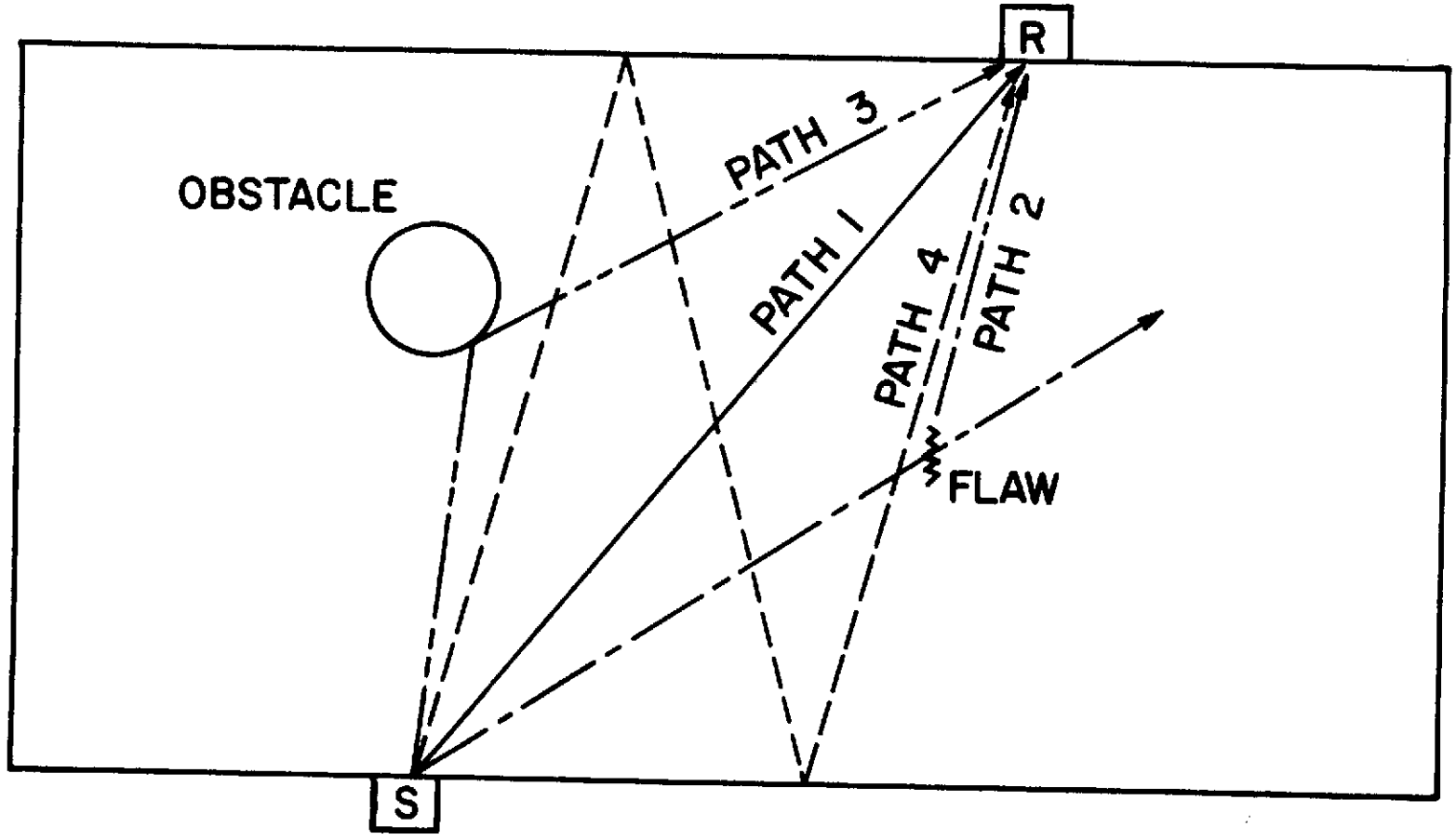

Figure 1.- Transmission of ultrasound by way of multiple paths.

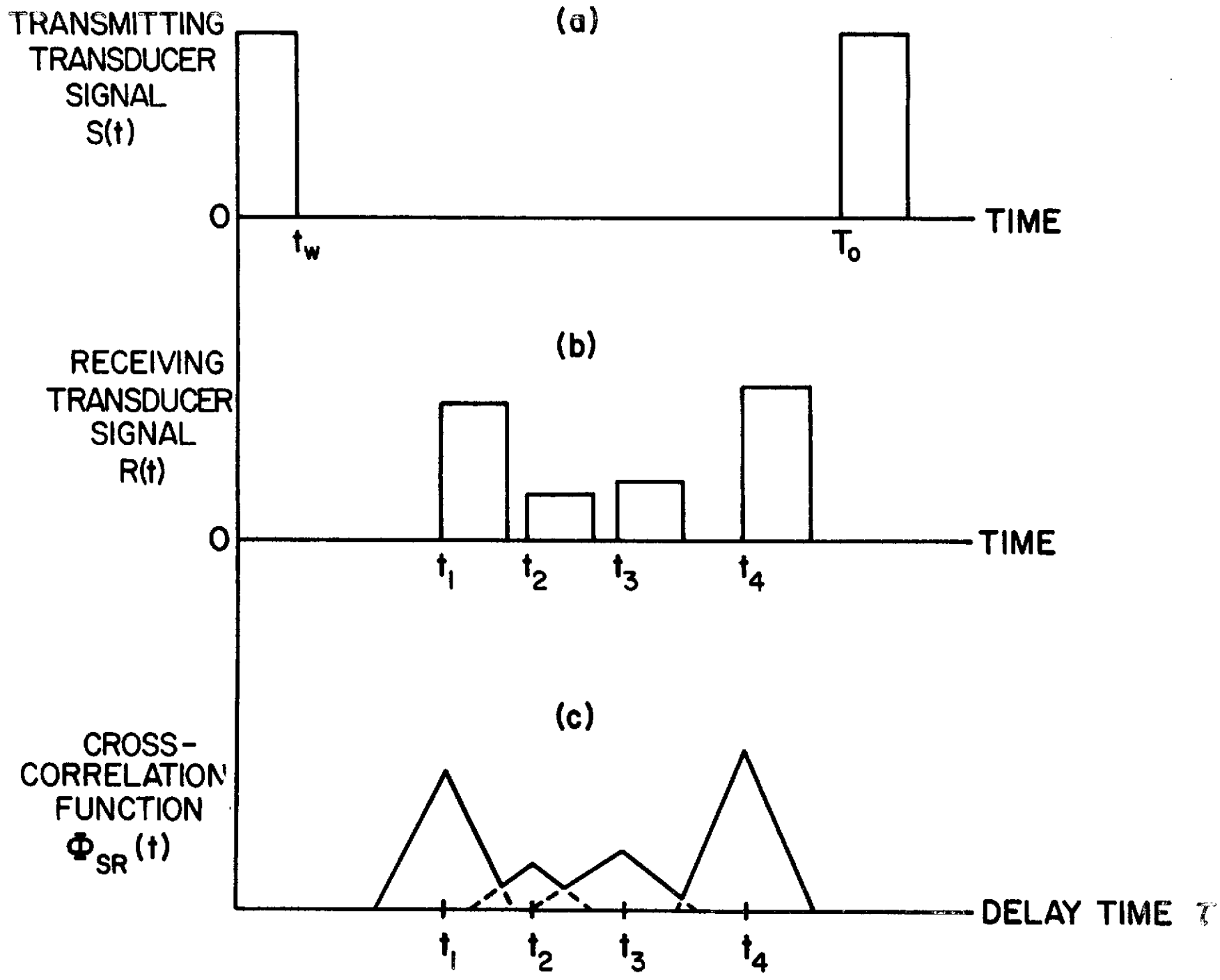

Figure 2.- Demodulated ultrasonic signals at the transmitting and receiving transducers and their cross-correlation (not to scale).

Legend to figure 3:

1. Electronic counter: Hewlett-Packard Model 5303B.
2. Reference oscillator: Hewlett-Packard Model 651B.
3. Tone burst generator: Exact Model 7060.
4. RF power amplifier: Electronic Navigation Industries Model 350L.
5. VHF attenuator: Hewlett-Packard Model 355D.
6. Same as 5.
7. Dual amplifier: Hewlett-Packard Model 8447A.
8. Mixer: Hewlett-Packard Model 10514A.
9. Same as 8.
10. Preamplifier: Princeton Applied Research Model 113.
11. Same as 10.
12. Logarithmic attenuator: own design.
13. Piezoelectric transducer: Branson Z-101-CF 10 MHz 1/4 inch diameter.
14. Magnetic tape recorder: Bell and Howell Data Tape VR-37003.
15. Oscilloscope: Tektronix Type 547.
16. Same as 13.

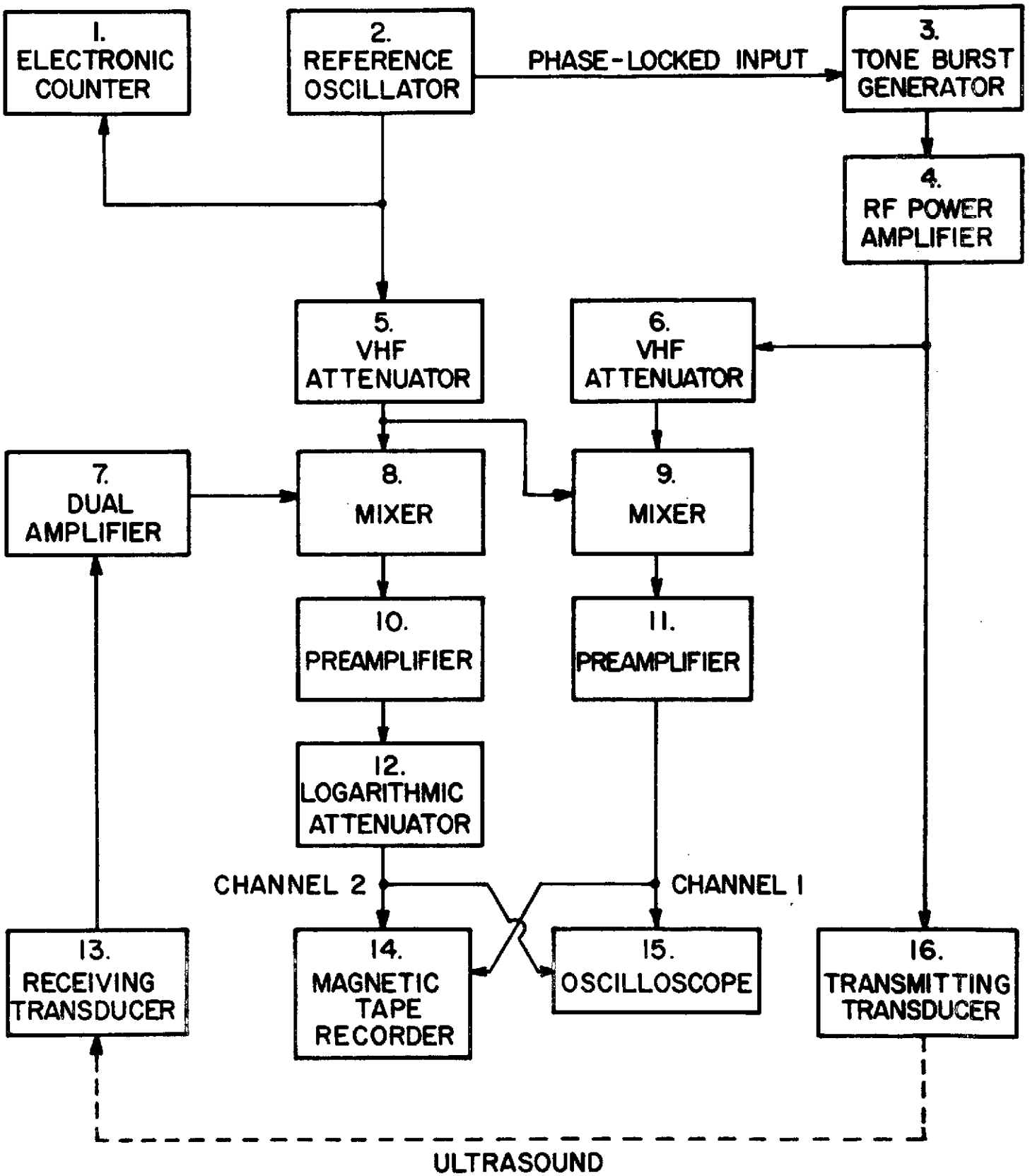

Figure 3.- Block diagram of the electronic system.

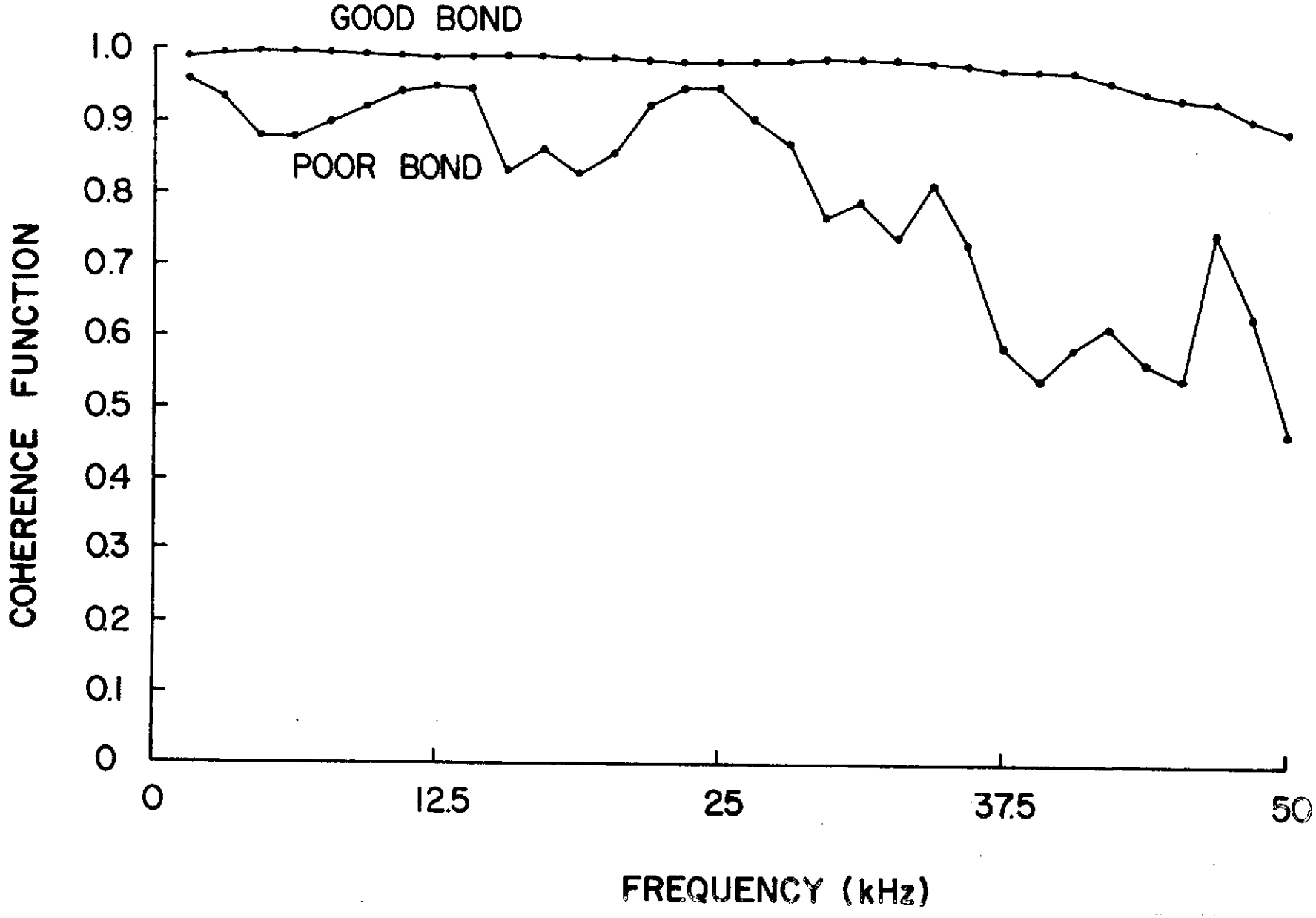

Figure 4.- Dependence of the coherence function upon the quality of the transducer bond.

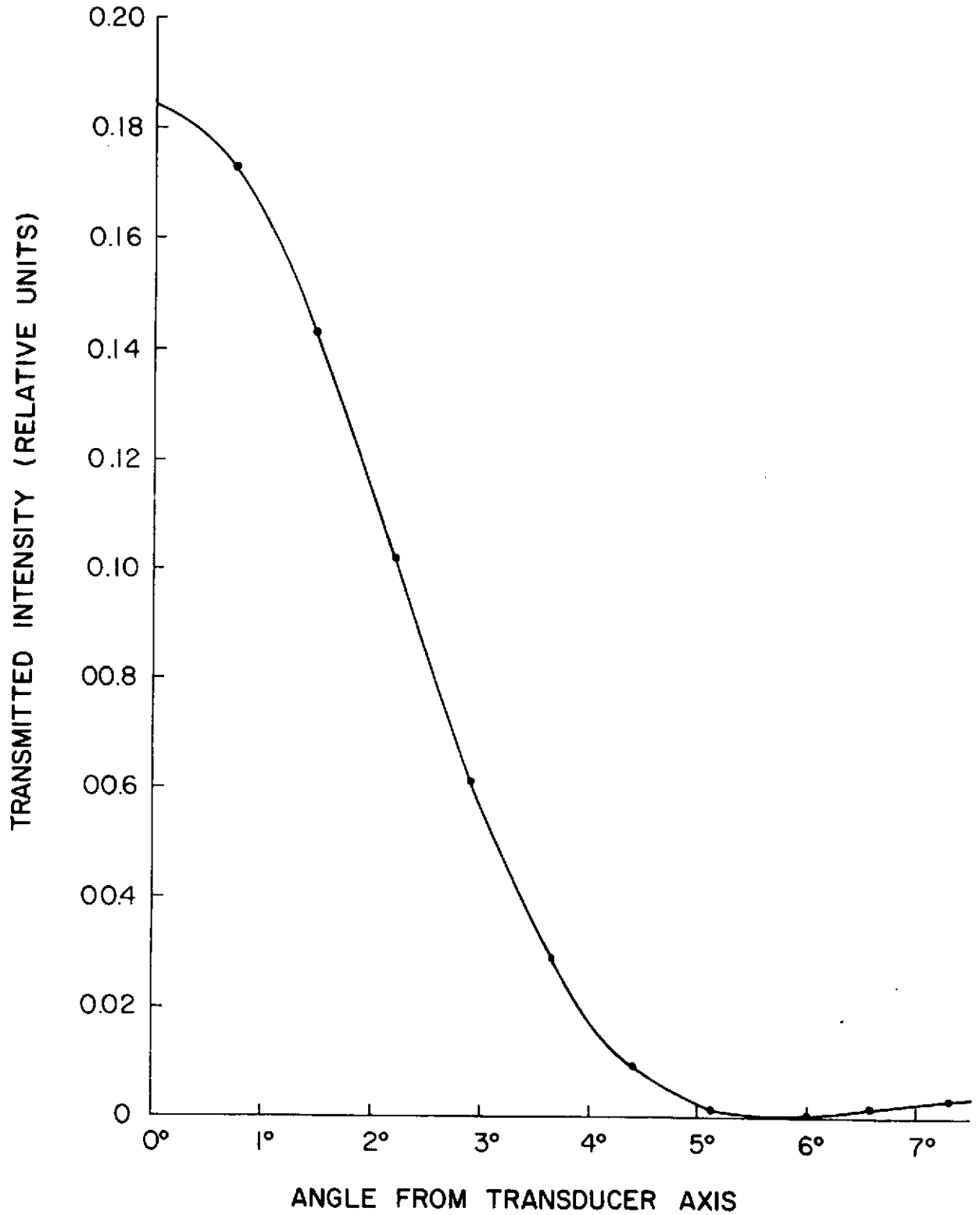

Figure 5.- Angular distribution of radiated intensity from the transmitting transducer.

Legend to figure 6:

1. Digital inputs:
   a. HP Model 2748A Tape Reader
   b. HP Model 2754B Heavy Duty Teletype (Teletype Corp.) with Interface
2. Keyboard: HP Model 5475A Control Unit
3. Analog-to-Digital Converter: HP Model 5466A
4. Display:
   a. HP Model H51-180A Oscilloscope
   b. HP Model 5460A Display Unit
5. Computer: HP Model 2100A (8K Memory)
6. X-Y Plotter: Moseley Model 2D2
7. Output: HP Model 2754B Heavy Duty Teletype (Teletype Corp.) with Interface
   a. Printout
   b. Punched tape

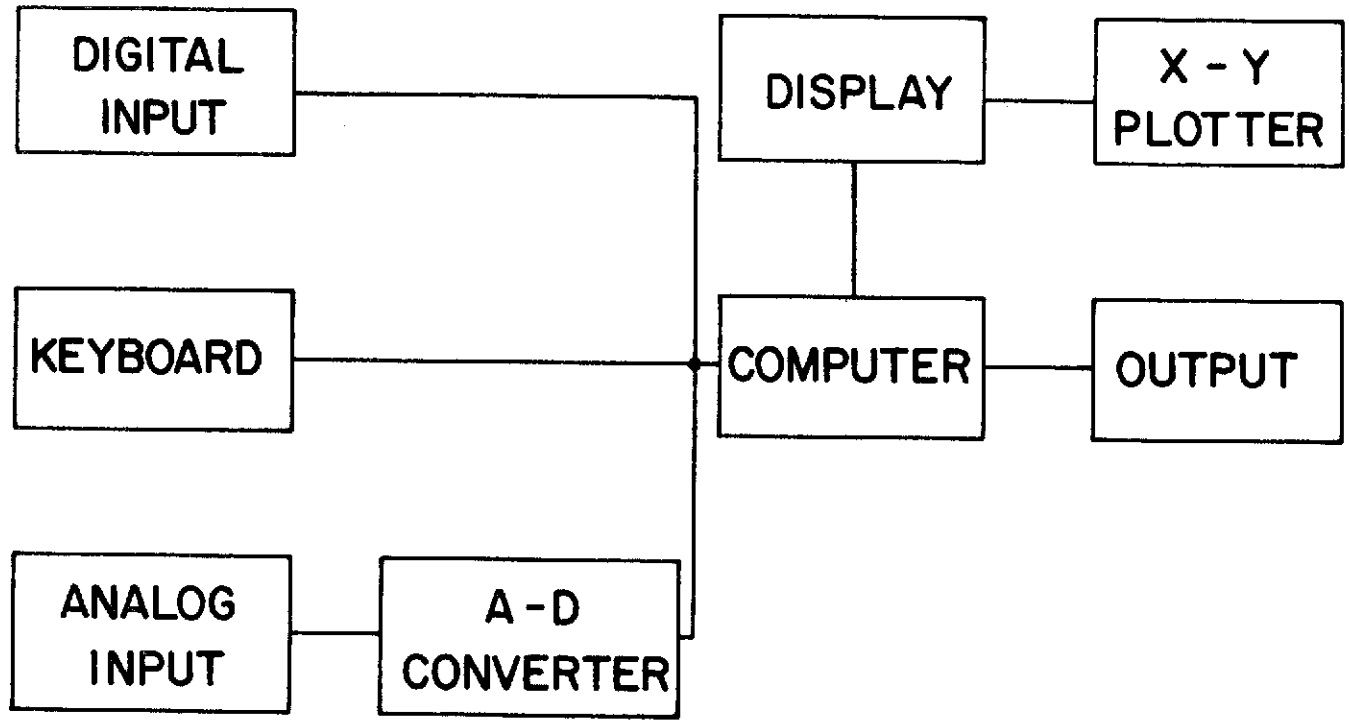

Figure 6.- Basic components of the Fourier analyzer system.

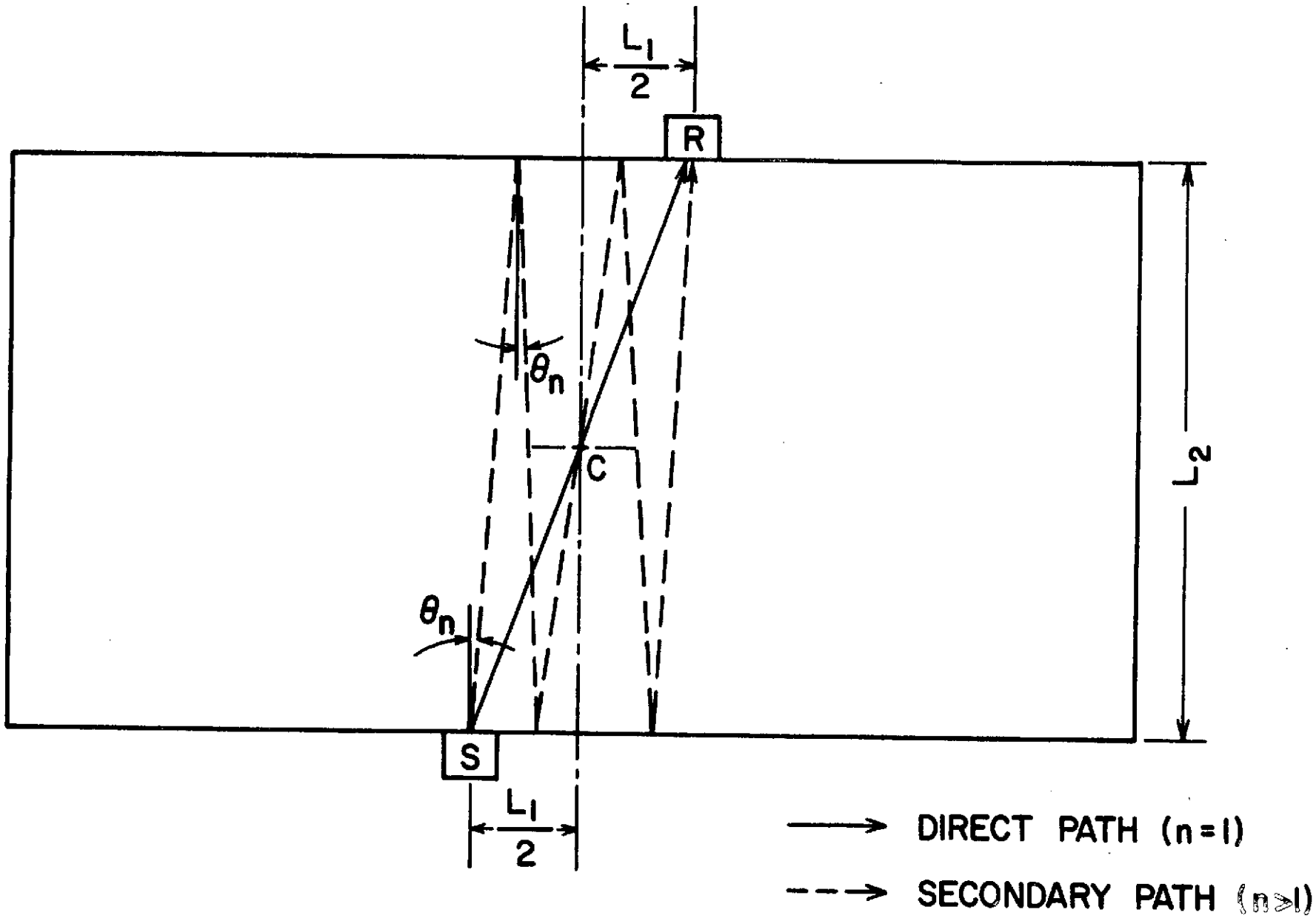

Figure 7.- Acoustical paths for the principal series of pulses.

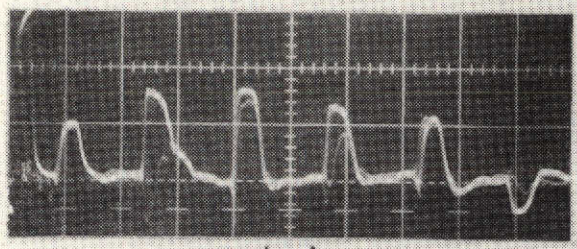

(a)

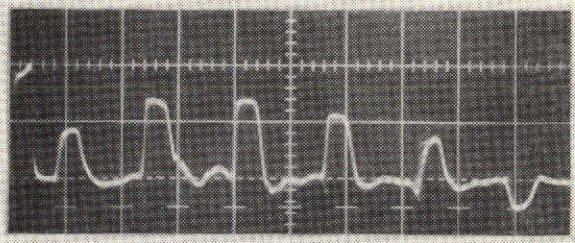

(f)

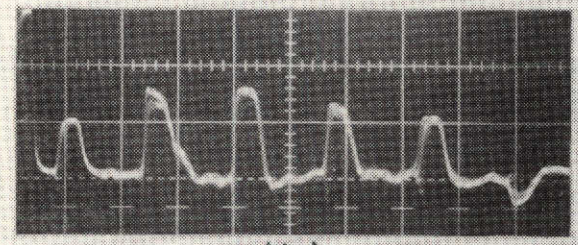

(b)

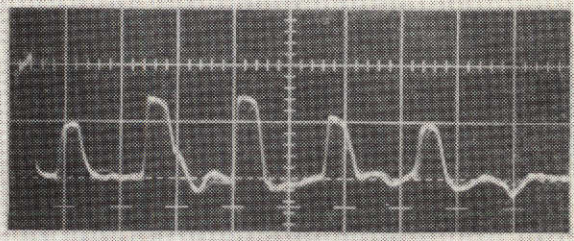

(g)

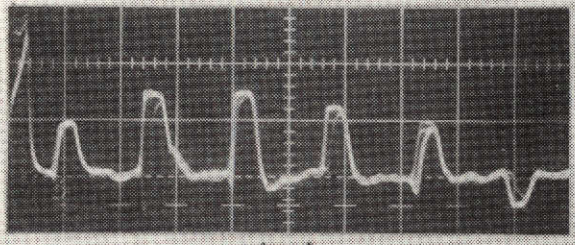

(c)

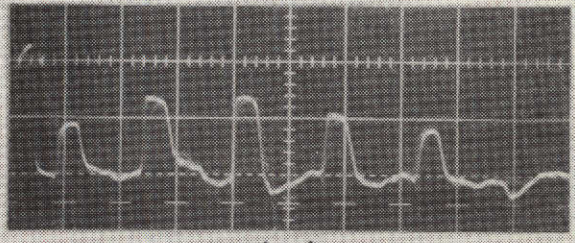

(h)

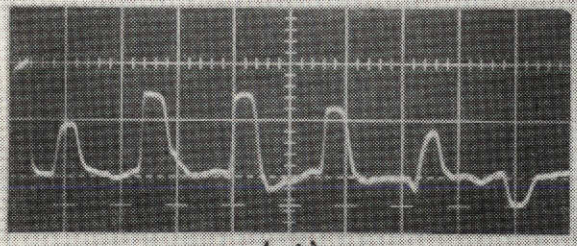

(d)

(i)

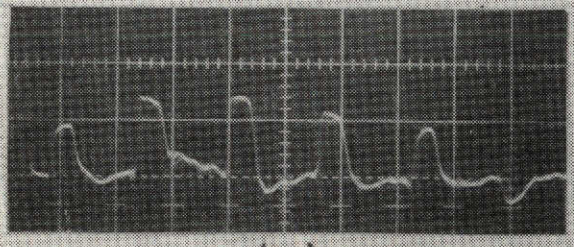

(e)

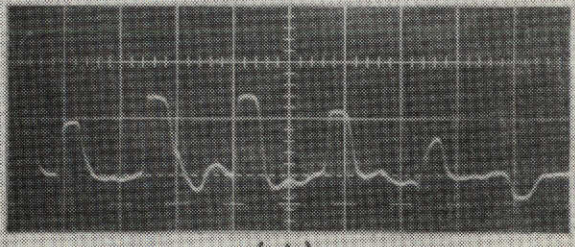

(j)

Figure 8.- Oscillcscope traces of the transmitted and received pulses of plate 10 for different hole diameters. The transmitted pulse is the first pulse on the left. Horizontal scale: 50 μsec/div. Vertical scale: 0.5 V/div (transmitted) and 0.1 V/div (received, approximately logarithmic). Hole diameters in mils: (a) no hole, (b) 13.5, (c) 21, (d) 28, (e) 35, (f) 40, (g) 52, (h) 70, (i) 82, (j) 98, (k) 110, (l) 128.5, (m) 149.5, (n) 161, (o) 180, (p) 193.5, (q) 205.5.

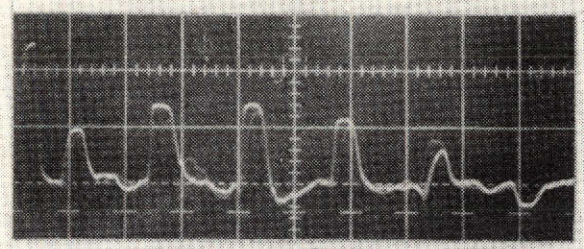

(k)

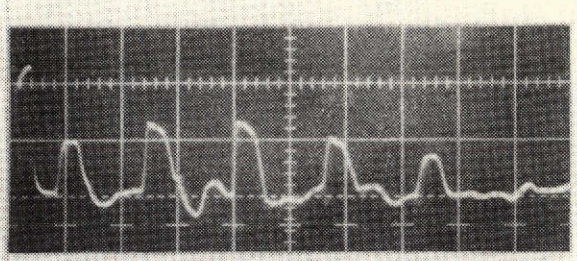

(o)

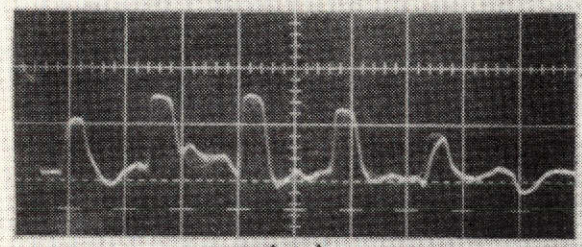

(l)

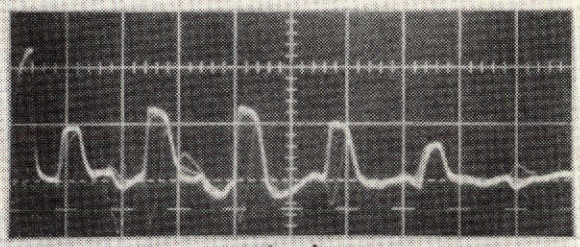

(p)

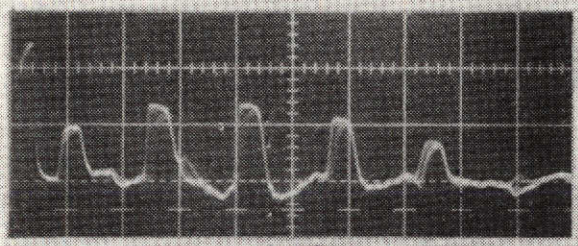

(m)

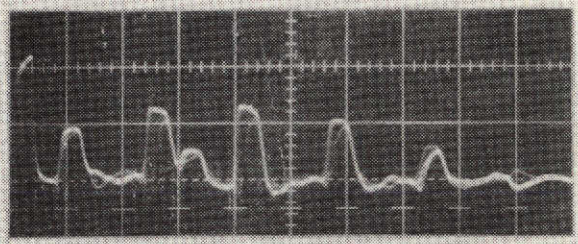

(q)

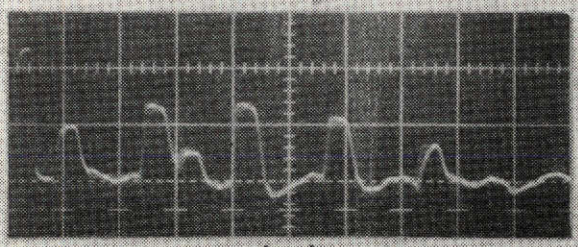

(n)

Figure 8.- Concluded.

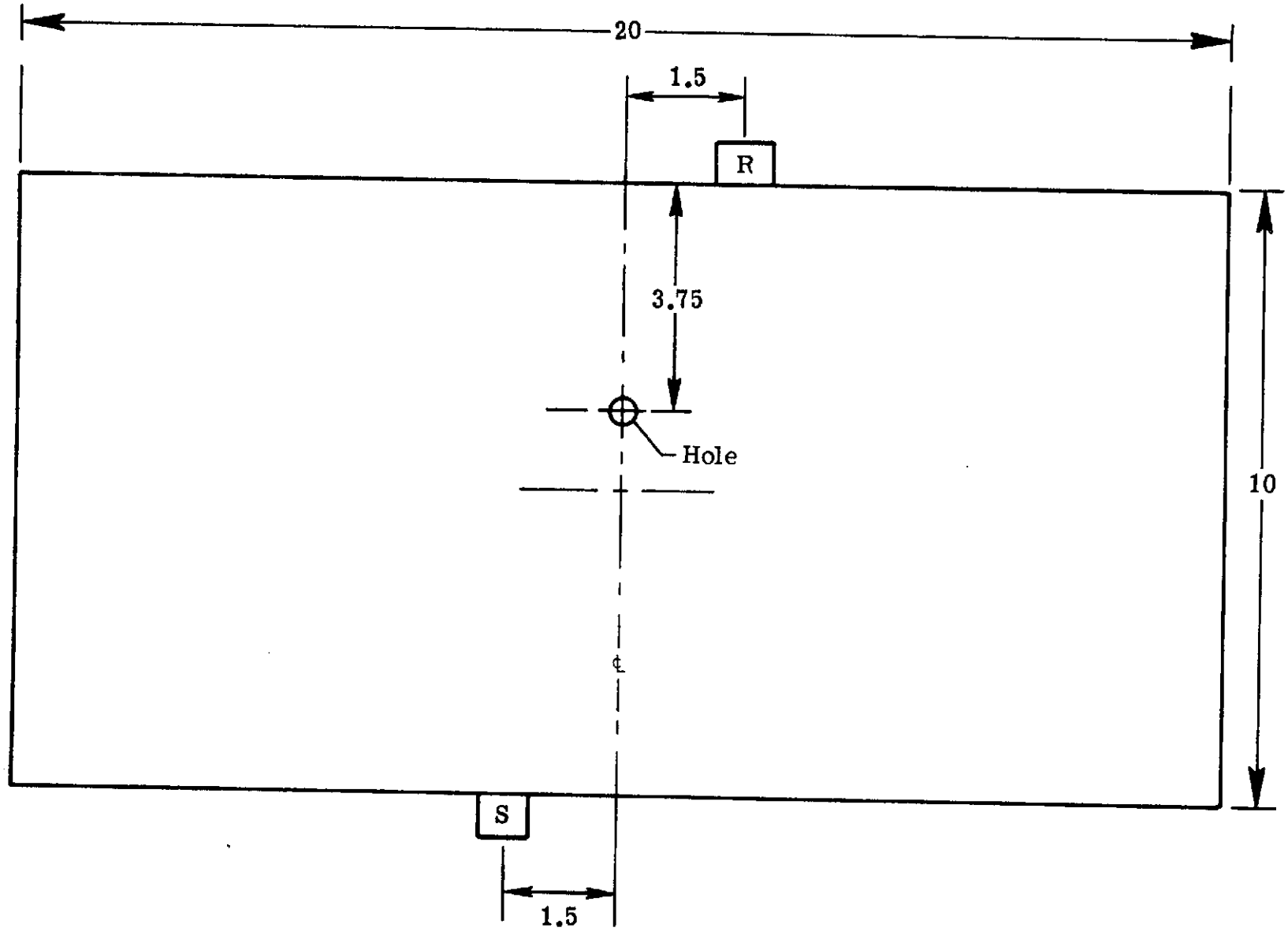

Figure 9.- Arrangement of transducers and hole on plate 10. All dimensions are in inches.

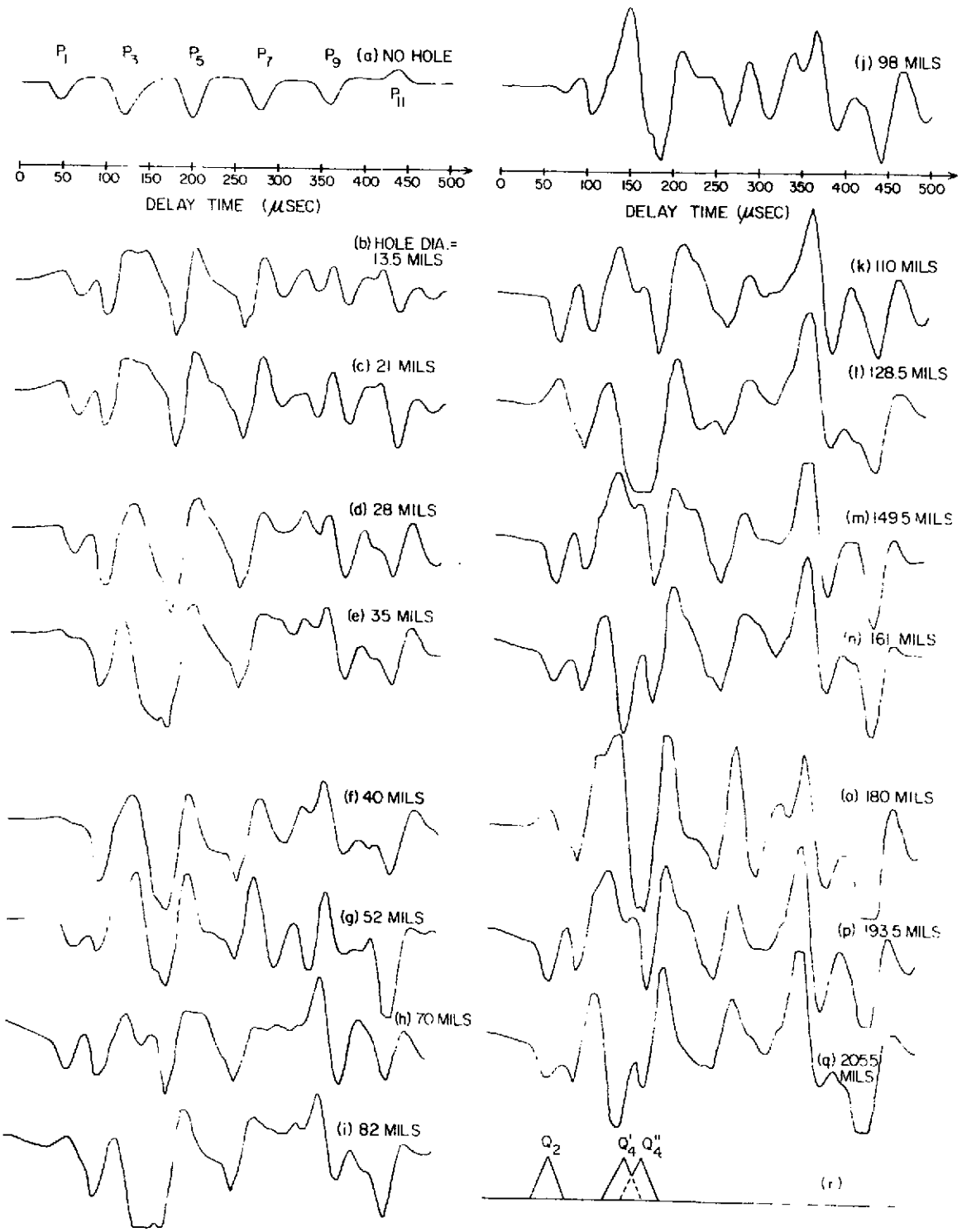

Figure 10.- Cross-correlograms of plate 10 for different hole diameters: (a) reference cross-correlogram (no hole, scale factor = 2×10^{-3}); (b)-(q) differential cross-correlograms (scale factor = 2×10^{-4}); (r) assumed cross-correlation triangles of the satellite pulses (not to scale).

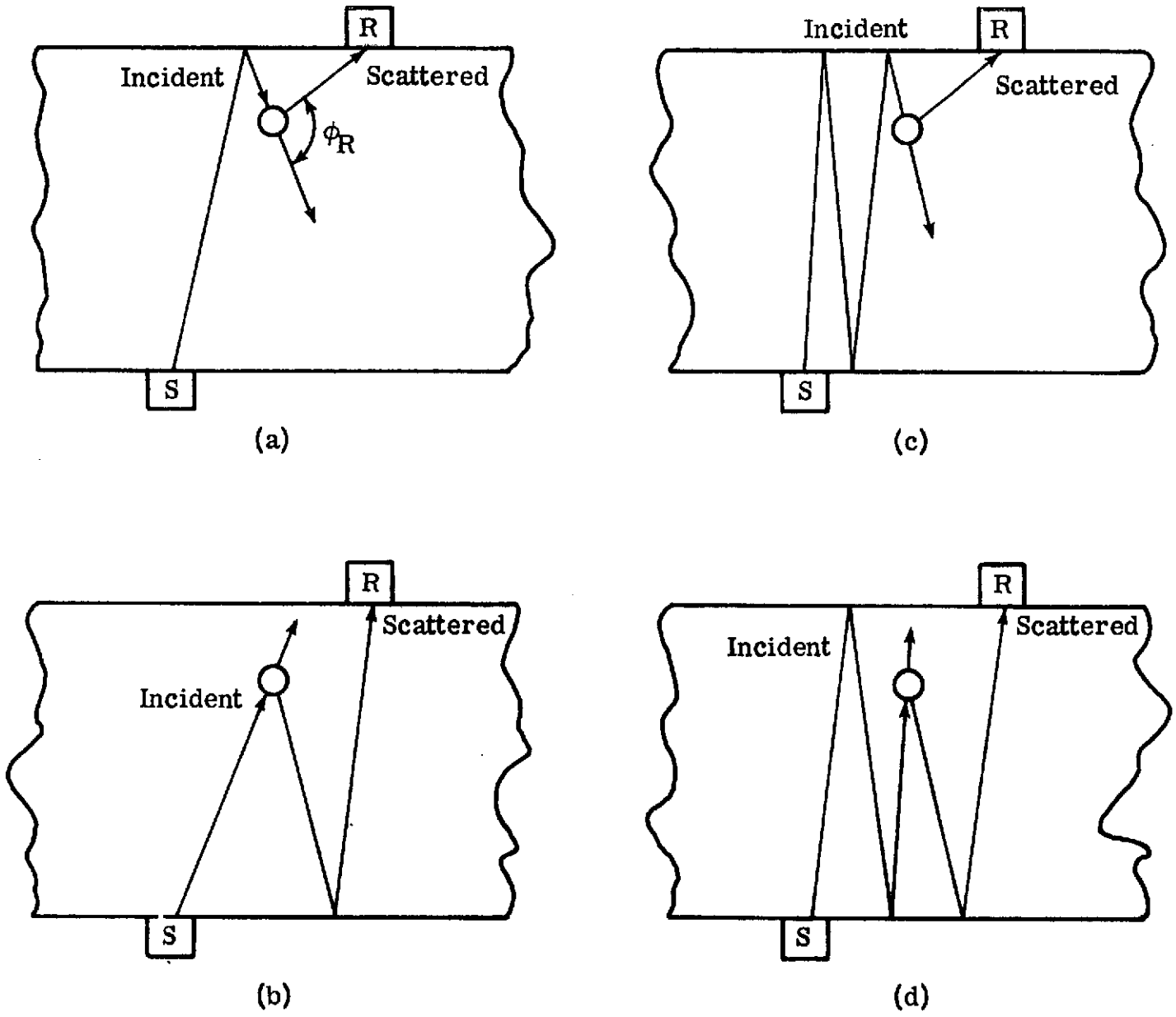

Figure 11.- Acoustical paths of the scattered (satellite) pulses: (a) Q_2', (b) Q_2'', (c) Q_4', (d) Q_4''.

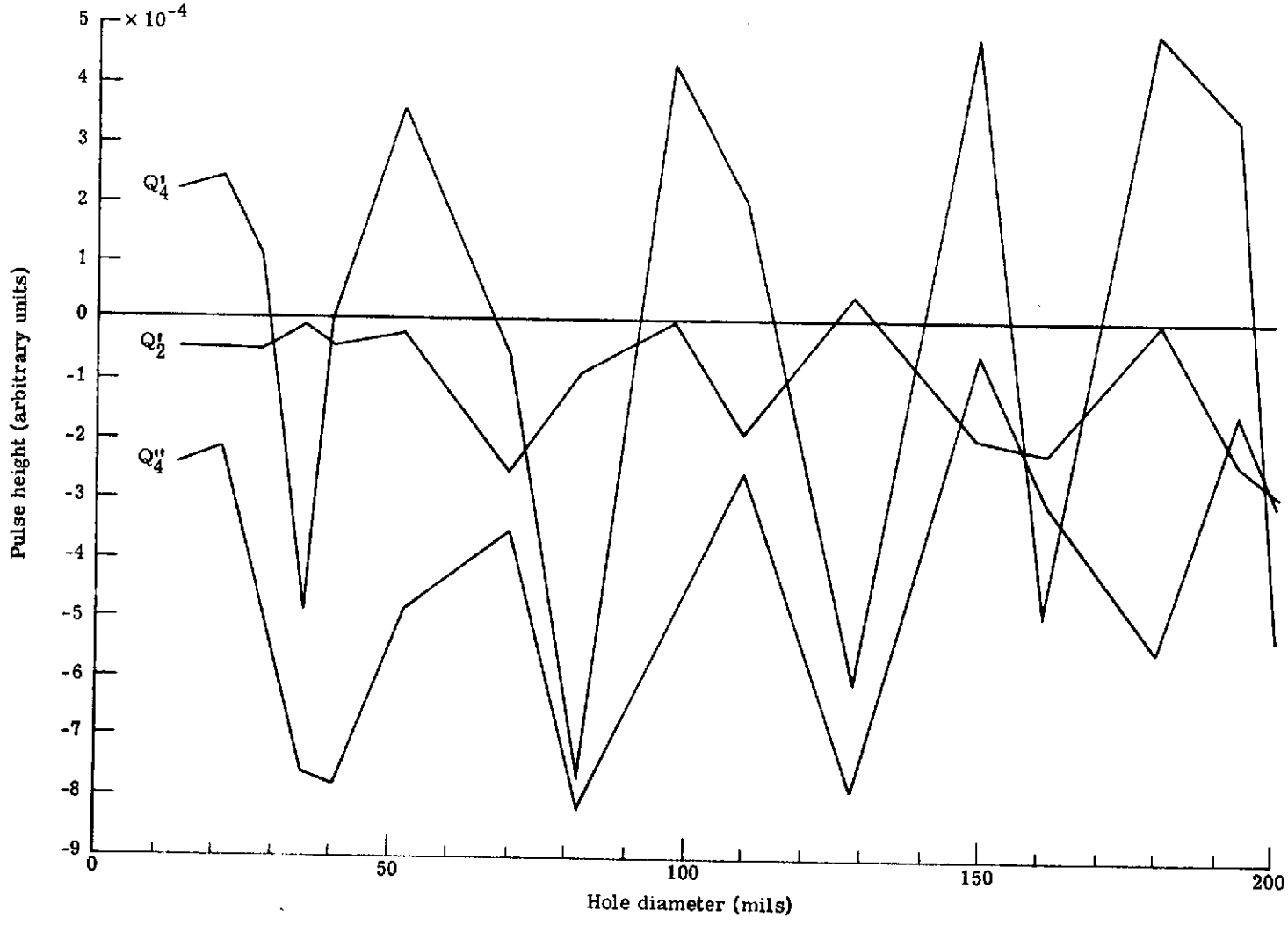

Figure 12.- Pulse height versus hole diameter for the satellite pulses of plate 10. The pulse height is obtained by integrating the differential cross-correlogram over the time interval of the corresponding triangle of figure 10(r).

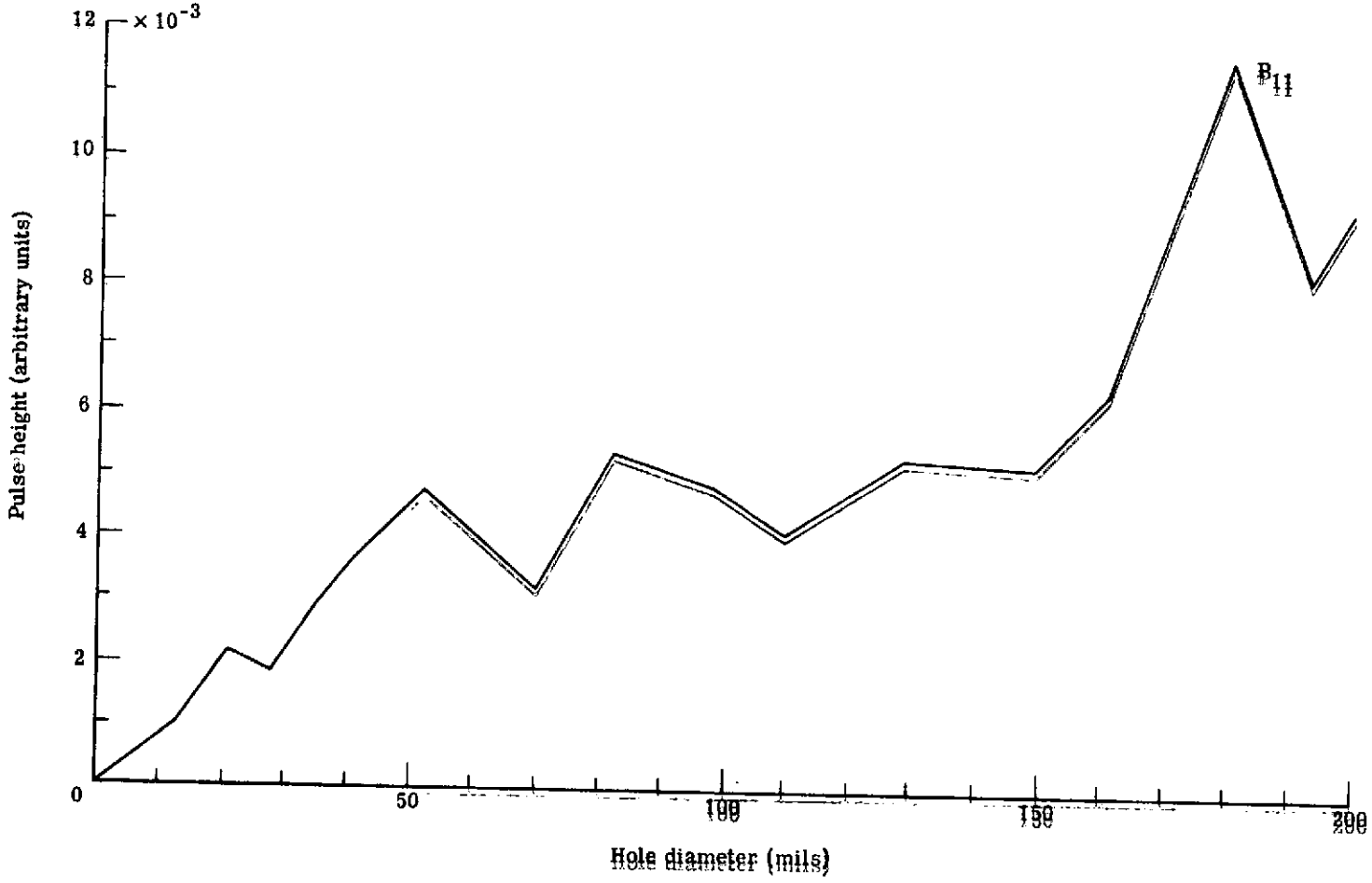

Figure 13.- Pulse height versus hole diameter of principal pulse P_{11} of plate 10. The pulse hieght is determined in the manner described in figure 12.

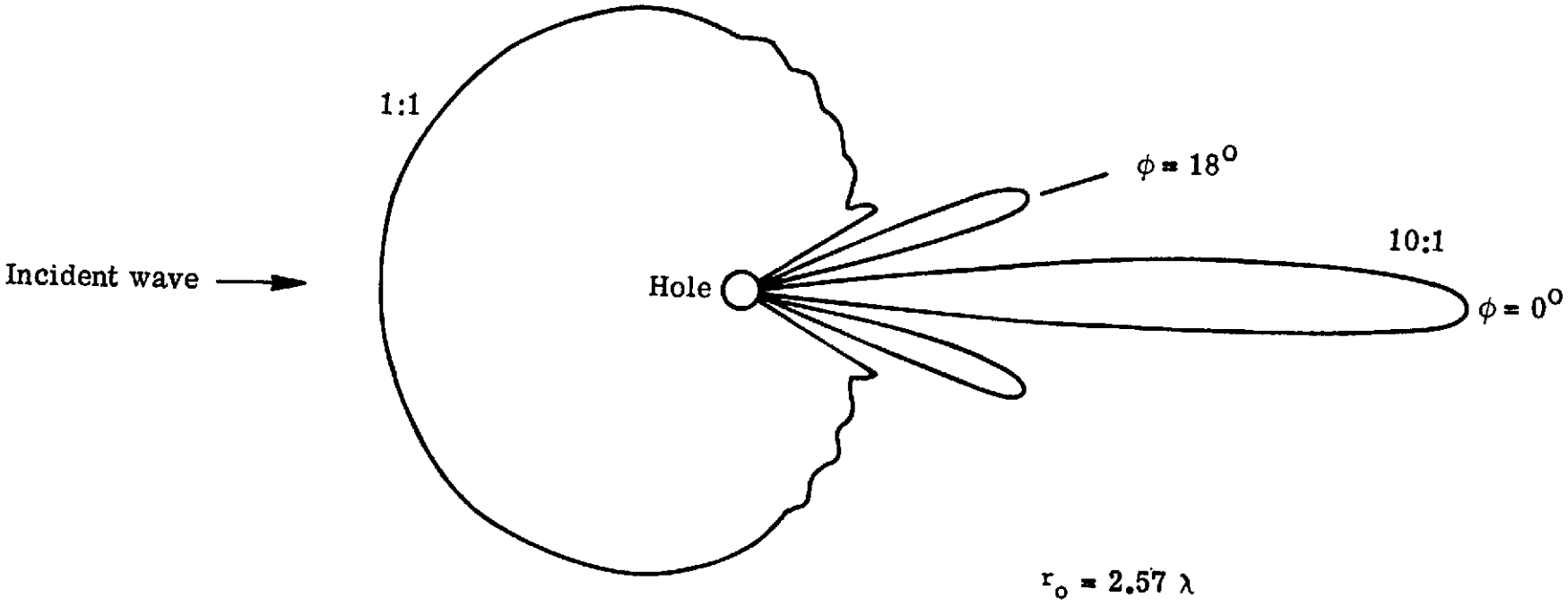

Figure 14.- Theoretical pattern of scattered intensity. Wavelength of ultrasound $\lambda = 0.04$ inch. Radius of hole $r_o = 0.10275$ inch. The forward lobe is reduced by a factor of 10:1.

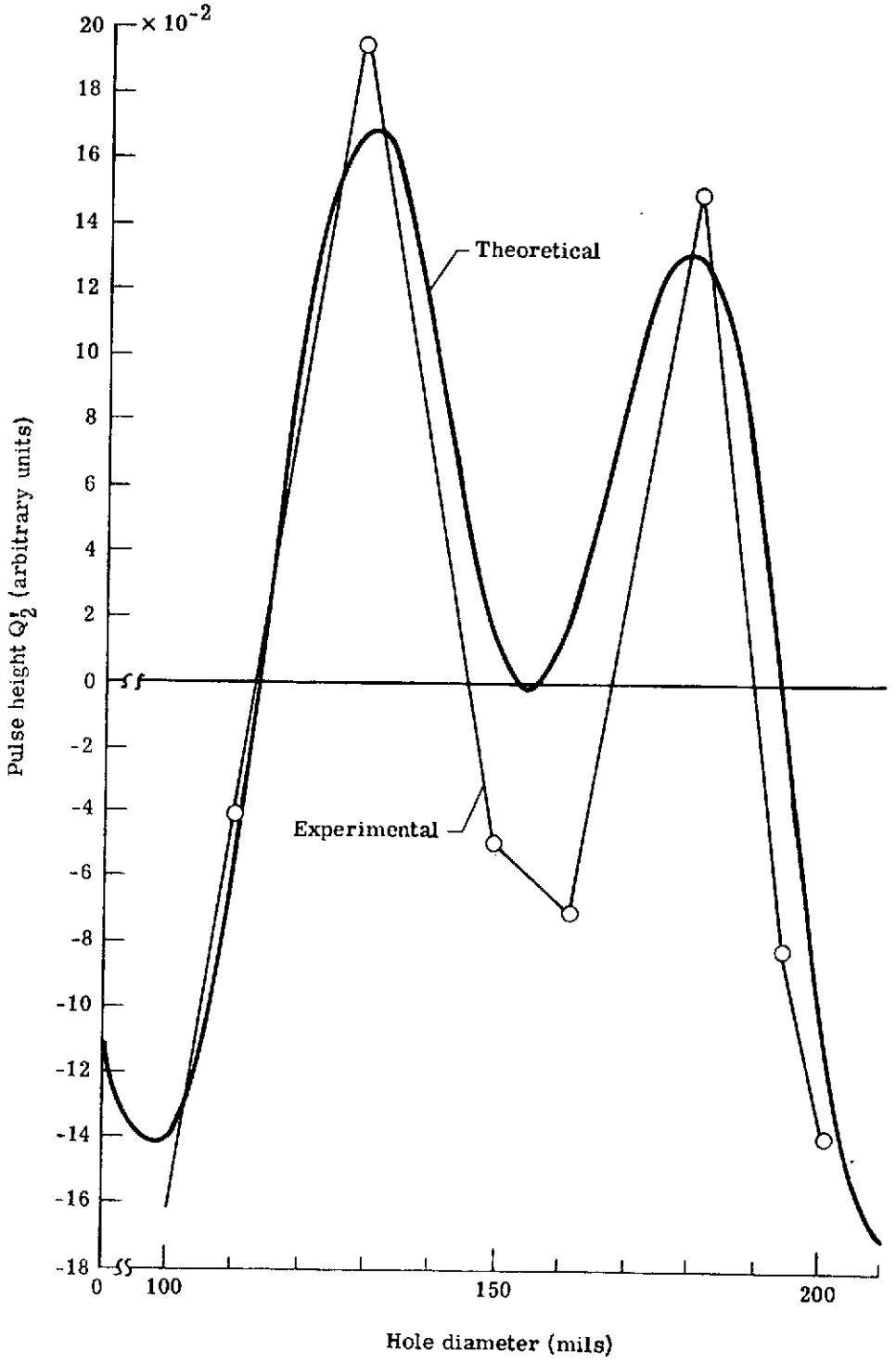

Figure 15.- Theoretical (heavy line) and experimental (light line) dependence of pulse height of Q_2' upon hole diameter. The theoretical curve was computed with the following values of the parameters: K = -4.984 arbitrary units, ϕ_o = 5.749 radians, ϕ_R = 2.652 radians, ϕ_1 = 0.0287 radians.

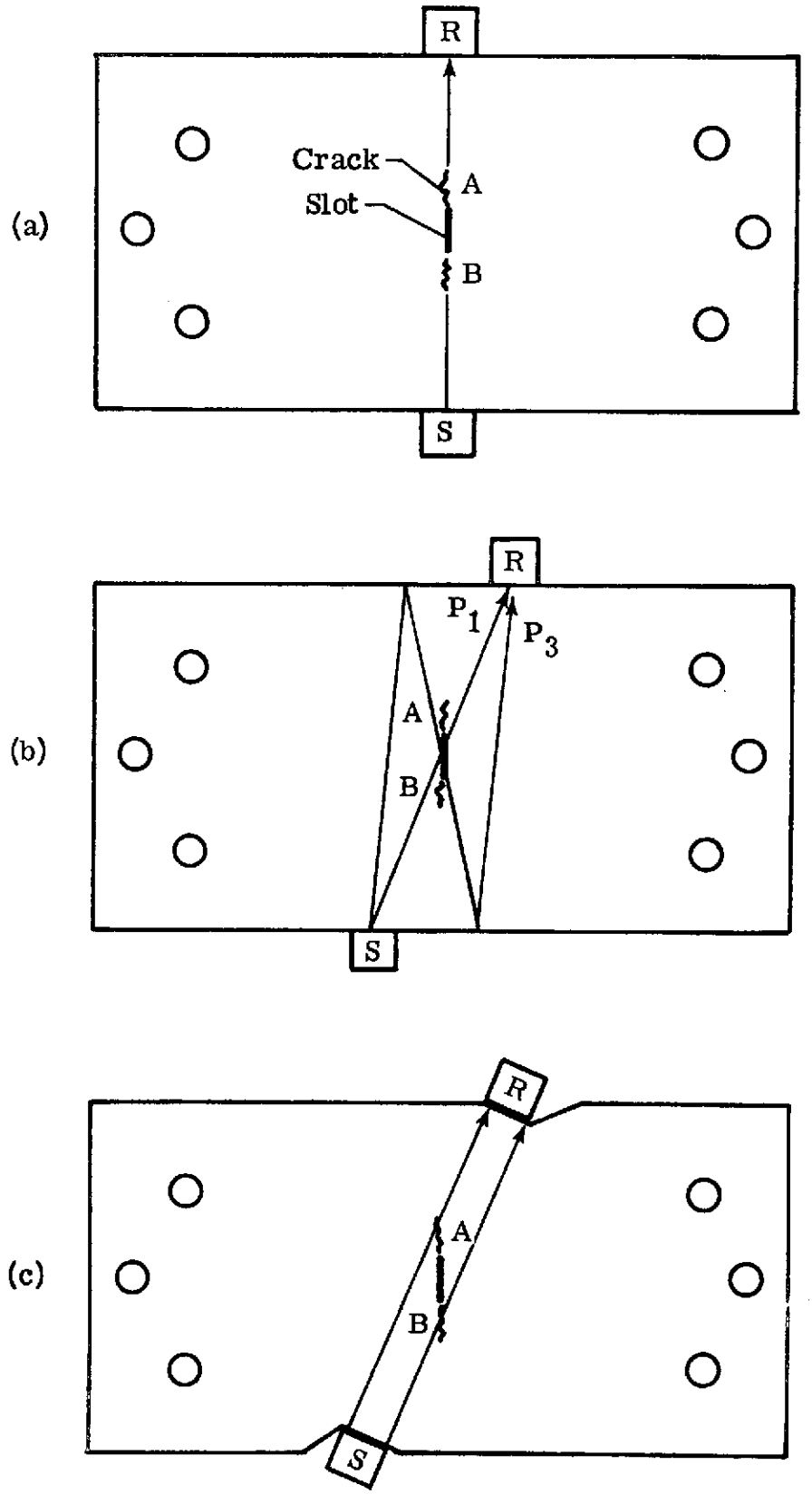

Figure 16.- Location of transducers S and R, slot A-B (0.015 inch wide by 1 inch long), grip holes, and fatigue-induced cracks in (a) plates 3 and 6, (b) plates 4 and 7, and (c) plate 5.

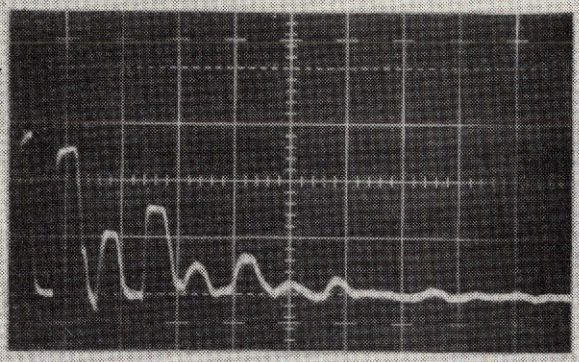

(a)

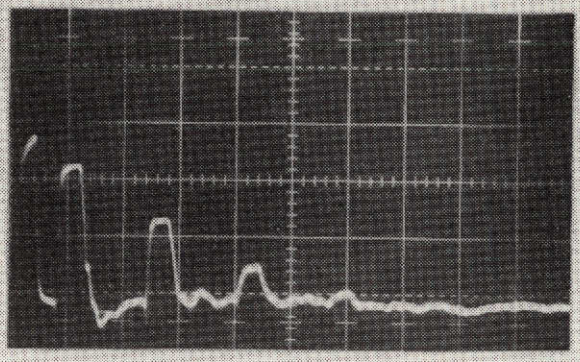

(b)

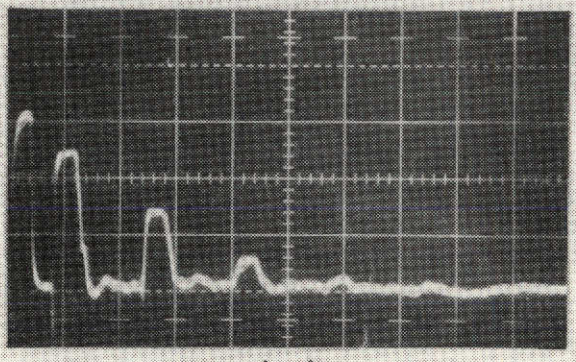

(c)

Figure 17.- Oscilloscope traces of the transmitted and received pulses of plate 6 after selected intervals of fatigue cycling: (a) prefatigue, (b) 30,200 cycles, (c) 90,500 cycles. Horizontal scale: 50 μsec/div. Vertical scale: 0.5 V/div (transmitted) and 0.1 V/div (received, approximately logarithmic).

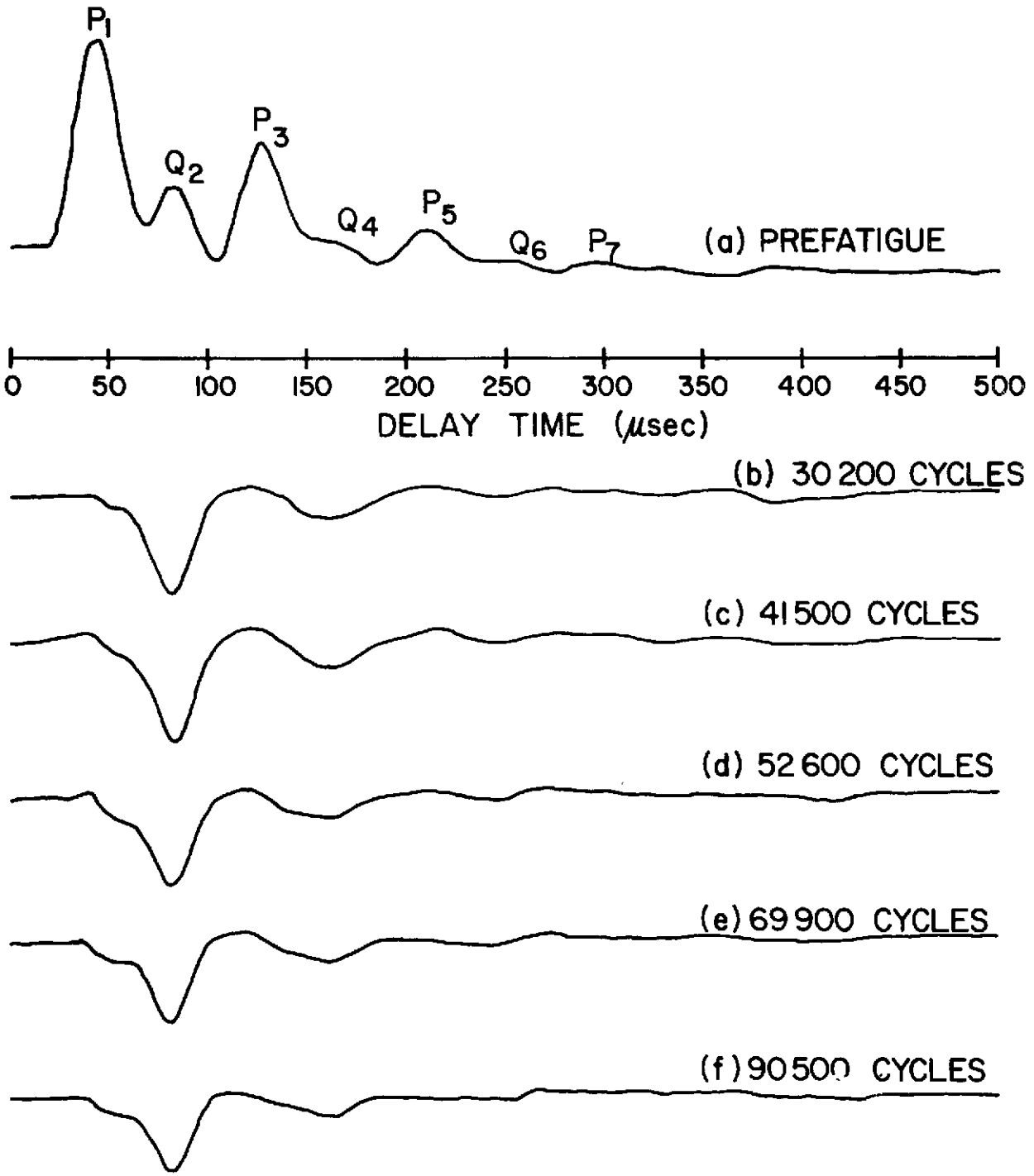

Figure 18.- Cross-correlograms of plate 6 after selected intervals of fatigue cycling: (a) reference cross-correlogram (prefatigue, scale factor = 2×10^{-3}); (b)-(f) differential cross-correlograms (scale factor = 2×10^{-3}).

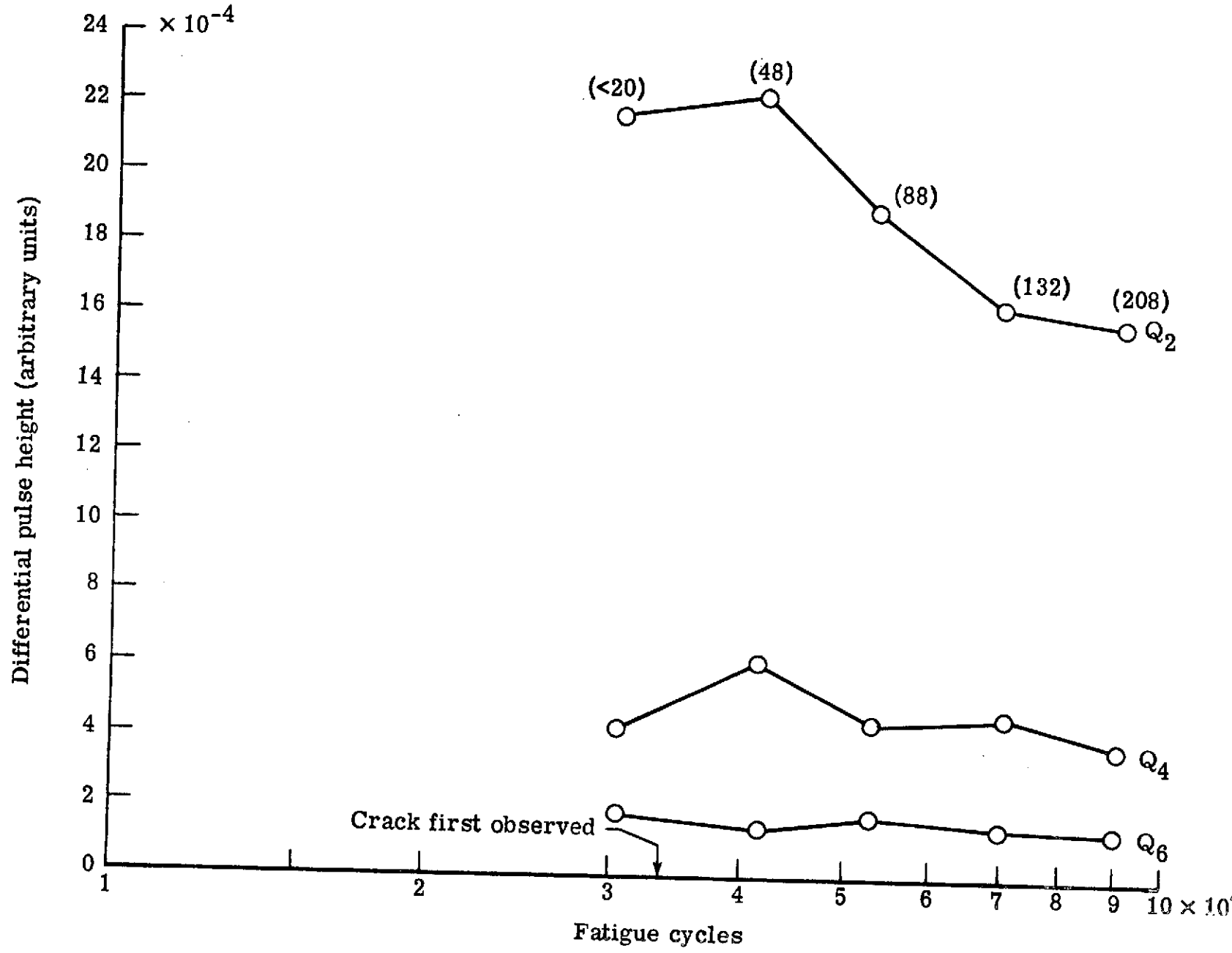

Figure 19.- Differential pulse height versus number of fatigue cycles of plate 6. Numbers in parentheses are measured crack lengths in mils.

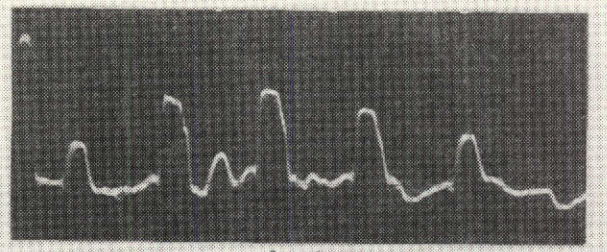

(a)

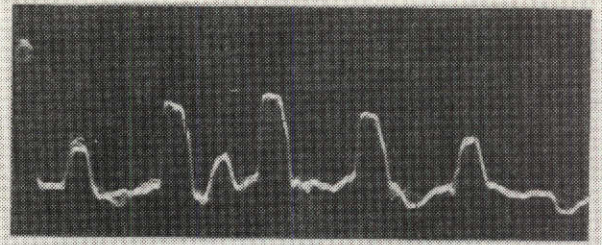

(b)

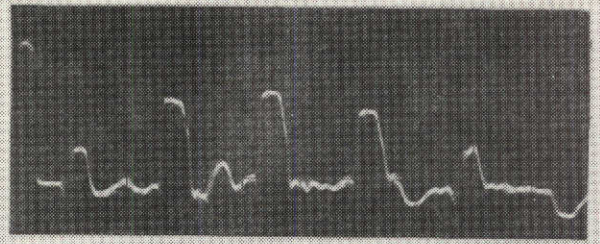

(c)

(d)

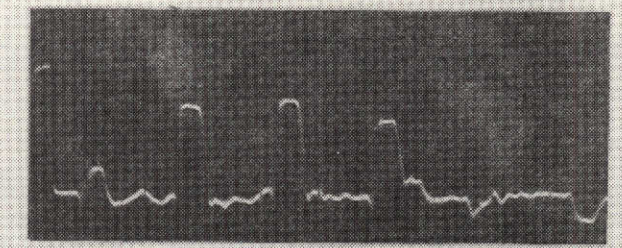

(e)

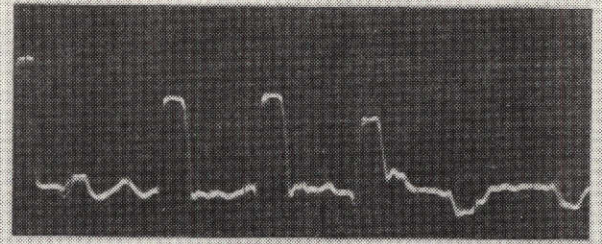

(f)

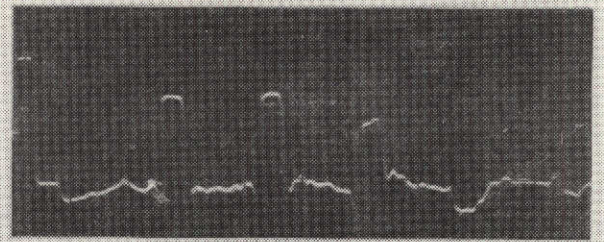

(g)

Figure 20.- Oscilloscope traces of the transmitted and received pulses of plate 7 after selected intervals of fatigue cycling: (a) prefatigue, (b) 20,400 cycles, (c) 30,300 cycles, (d) 32,800 cycles, (e) 62,000 cycles, (f) 82,200 cycles, (g) 121,700 cycles. Horizontal scale: 50 μsec/div. Vertical scale: 0.5 V/div (transmitted) and 0.1 V/div (received, approximately logarithmic).

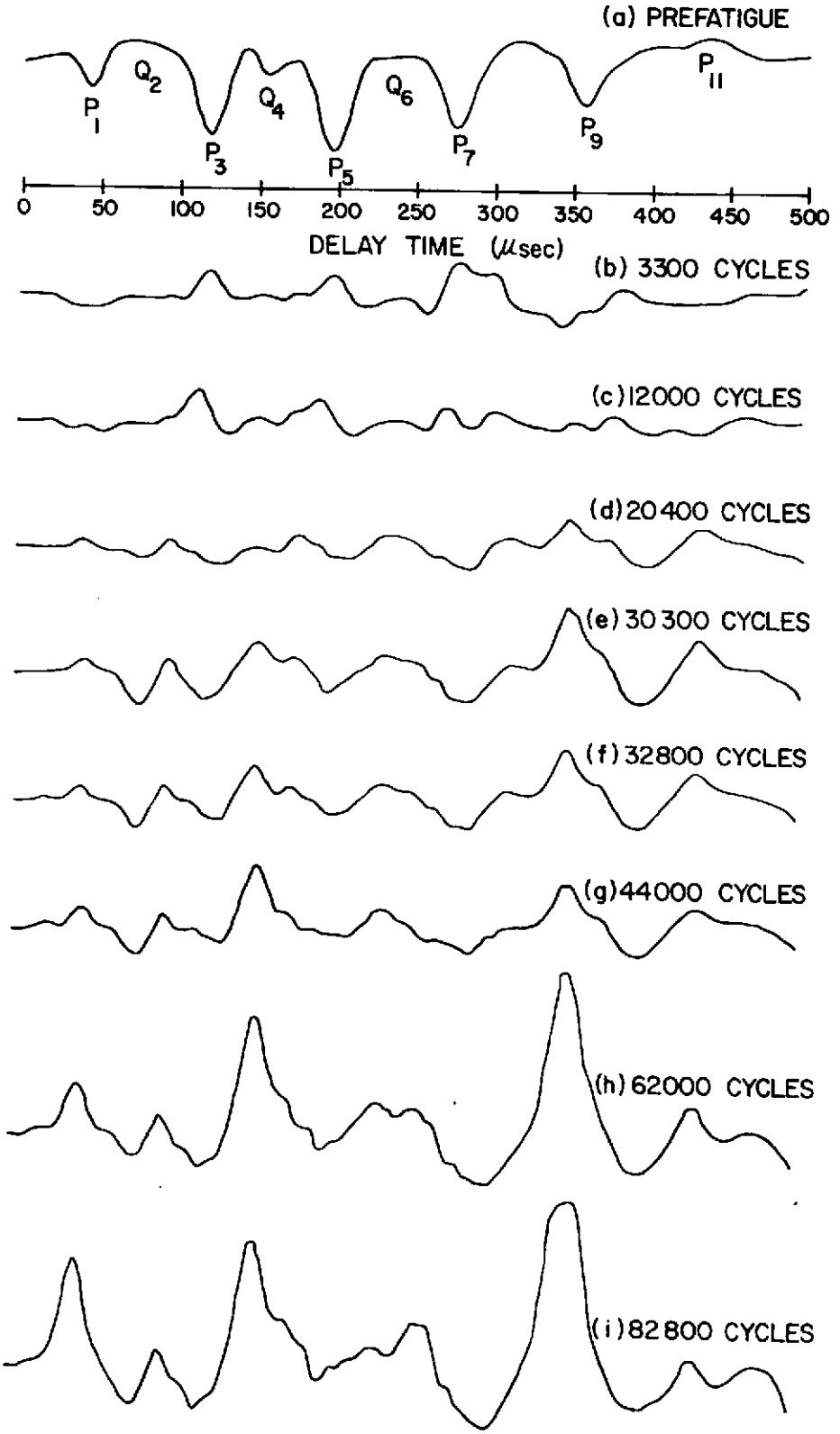

Figure 21.- Cross-correlograms of plate 7 after selected intervals of fatigue cycling: (a) reference cross-correlogram (prefatigue, scale factor = 2×10^{-3}); (b)-(i) differential cross-correlograms (scale factor = 5×10^{-4}).

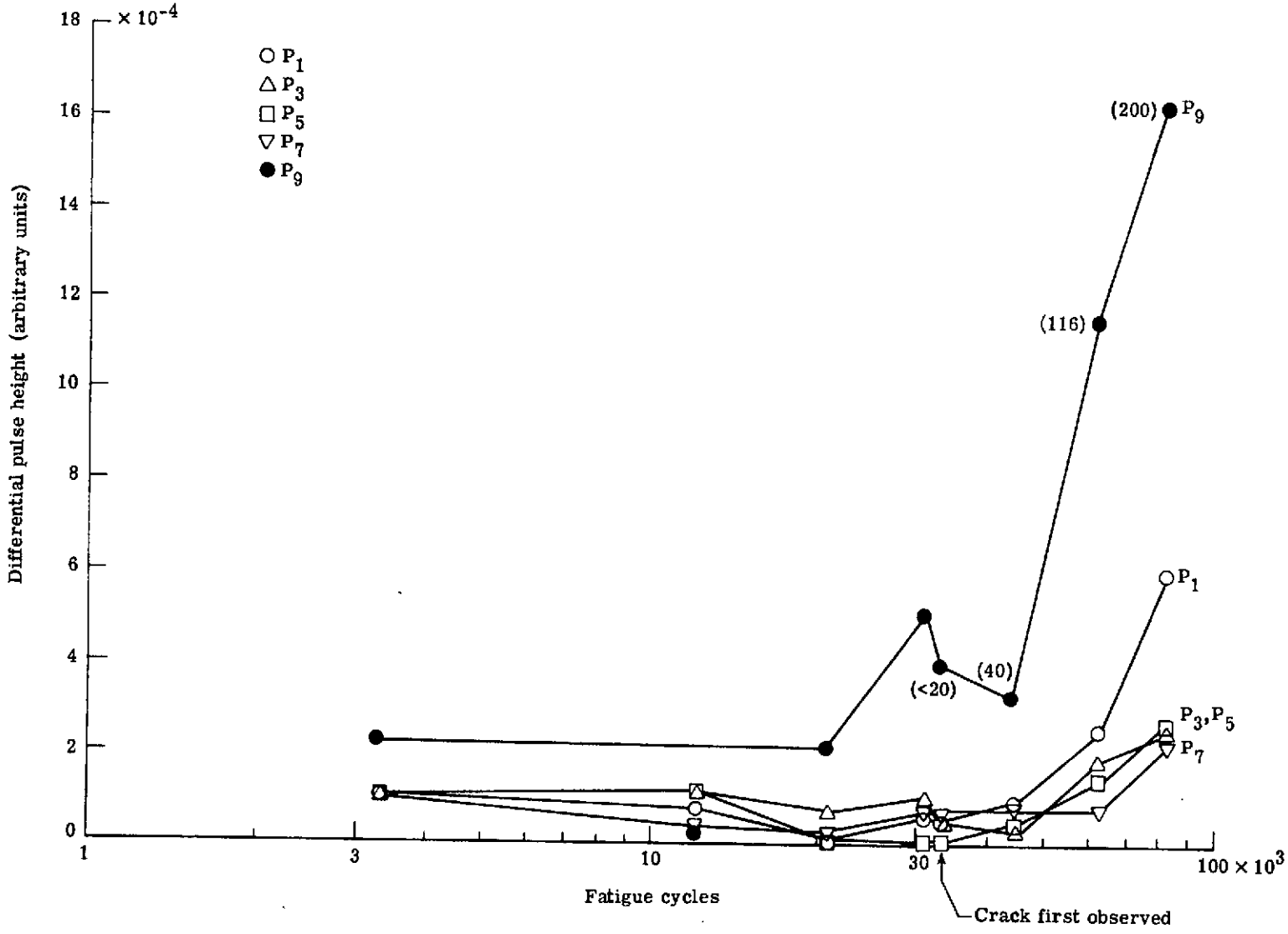

Figure 22.- Differential height of principal pulses versus number of fatigue cycles of plate 7. Numbers in parentheses are measured crack lengths in mils.

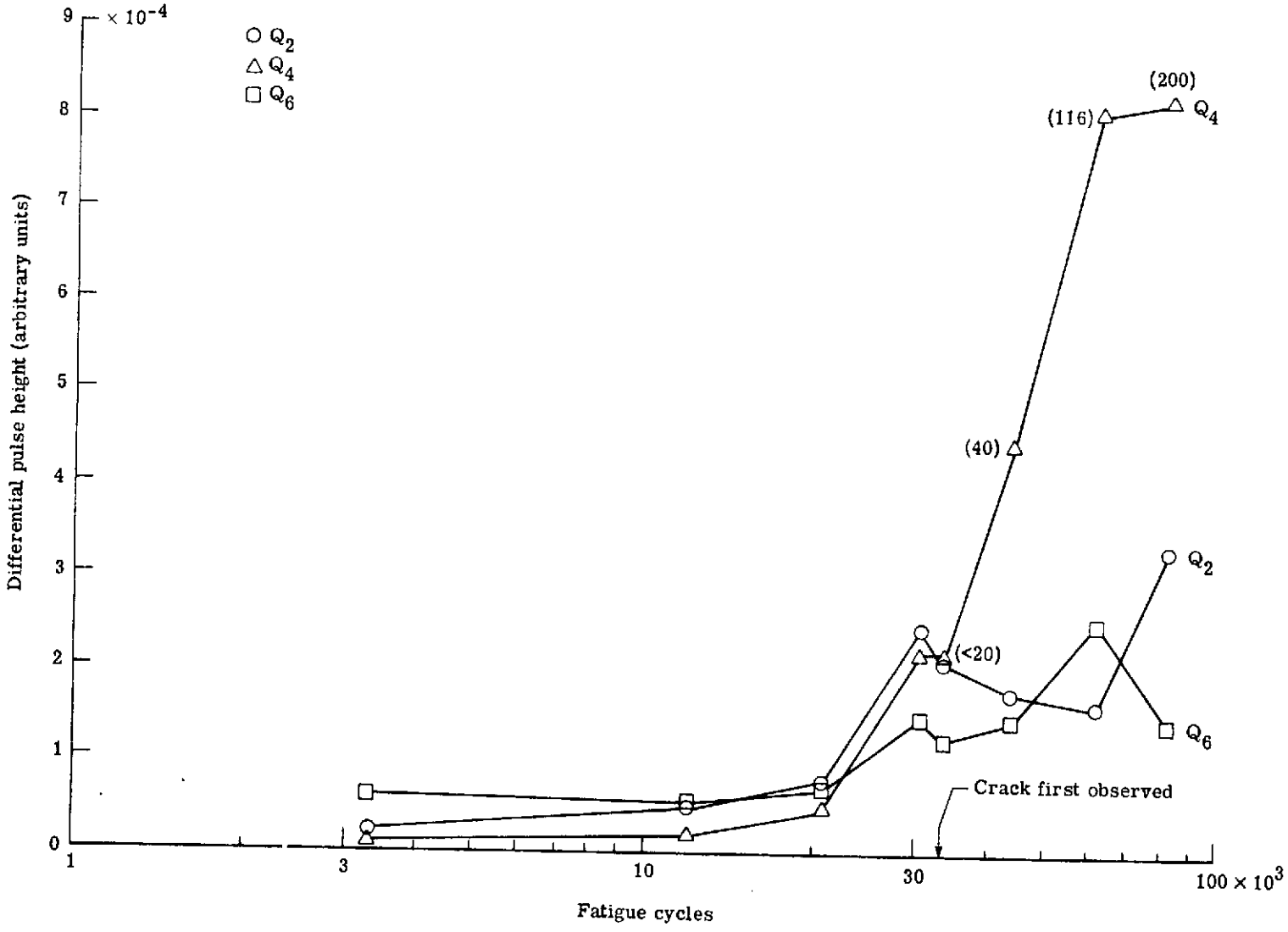

Figure 23.- Differential height of satellite pulses versus number of fatigue cycles of plate 7. Numbers in parentheses are measured crack lengths in mils.

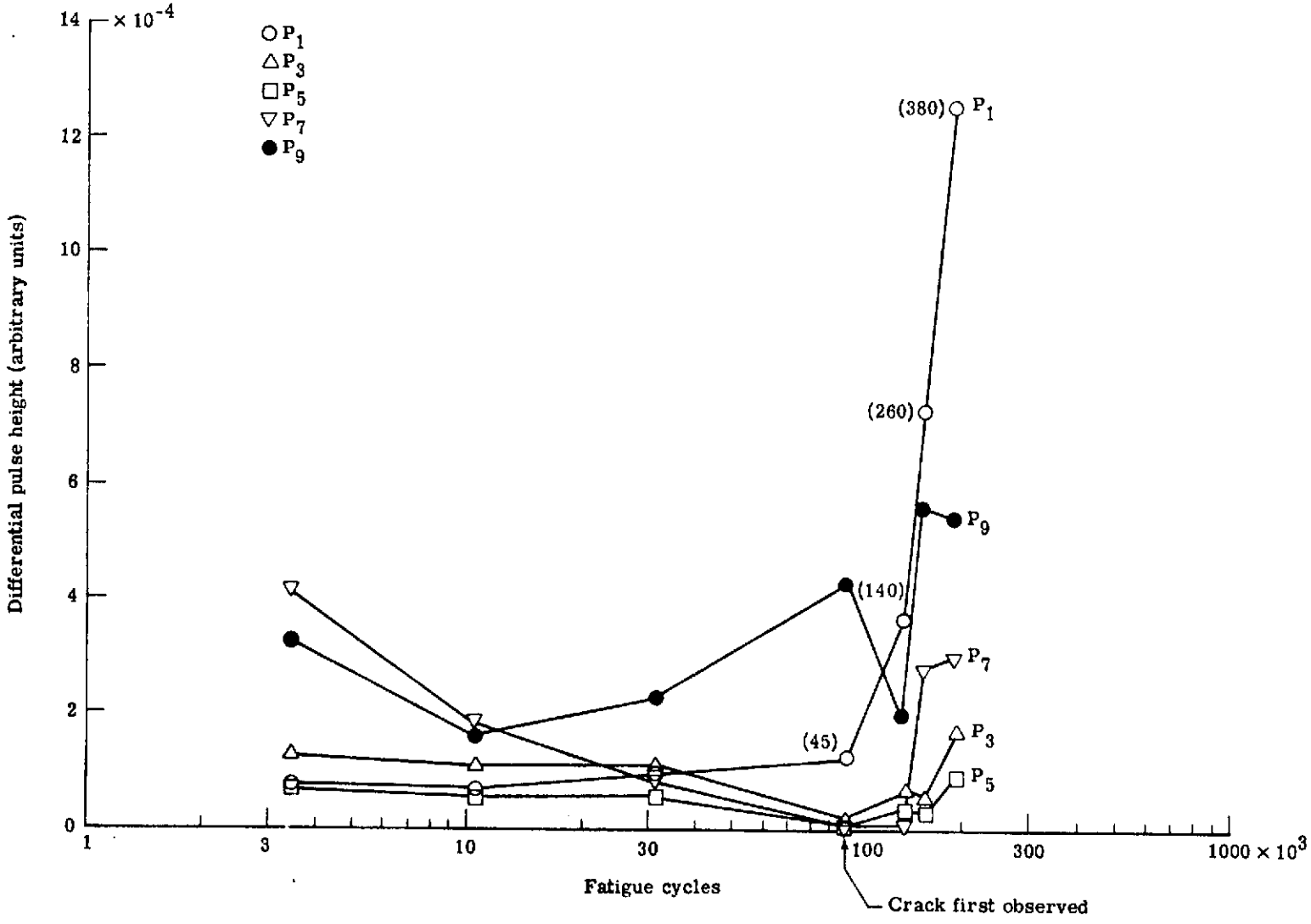

Figure 24.- Differential height of principal pulses versus number of fatigue cycles of plate 4. Numbers in parentheses are measured crack lengths in mils.

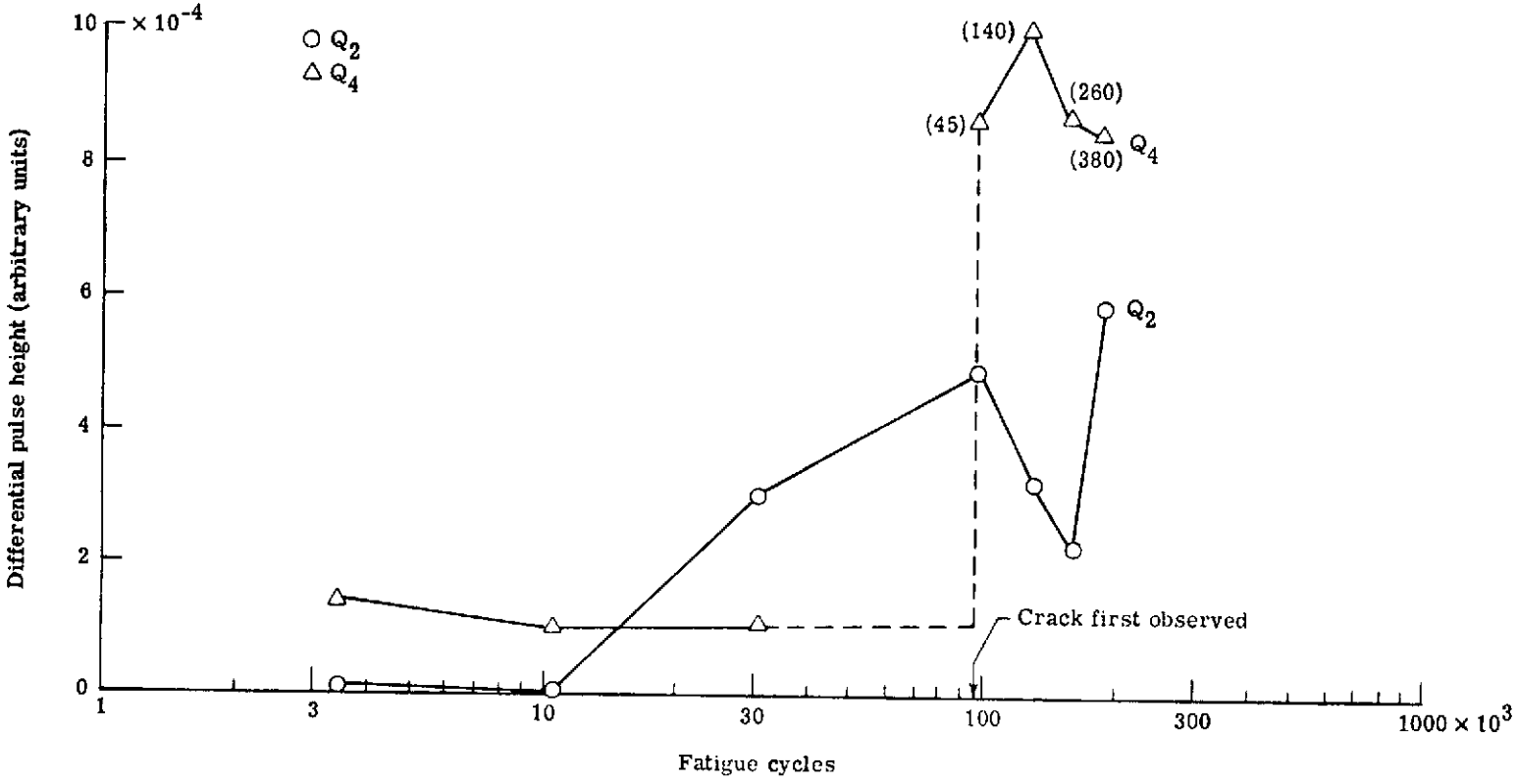

Figure 25.- Differential height of satellite pulses versus number of fatigue cycles of plate 4. Numbers in parentheses are measured crack lengths in mils.

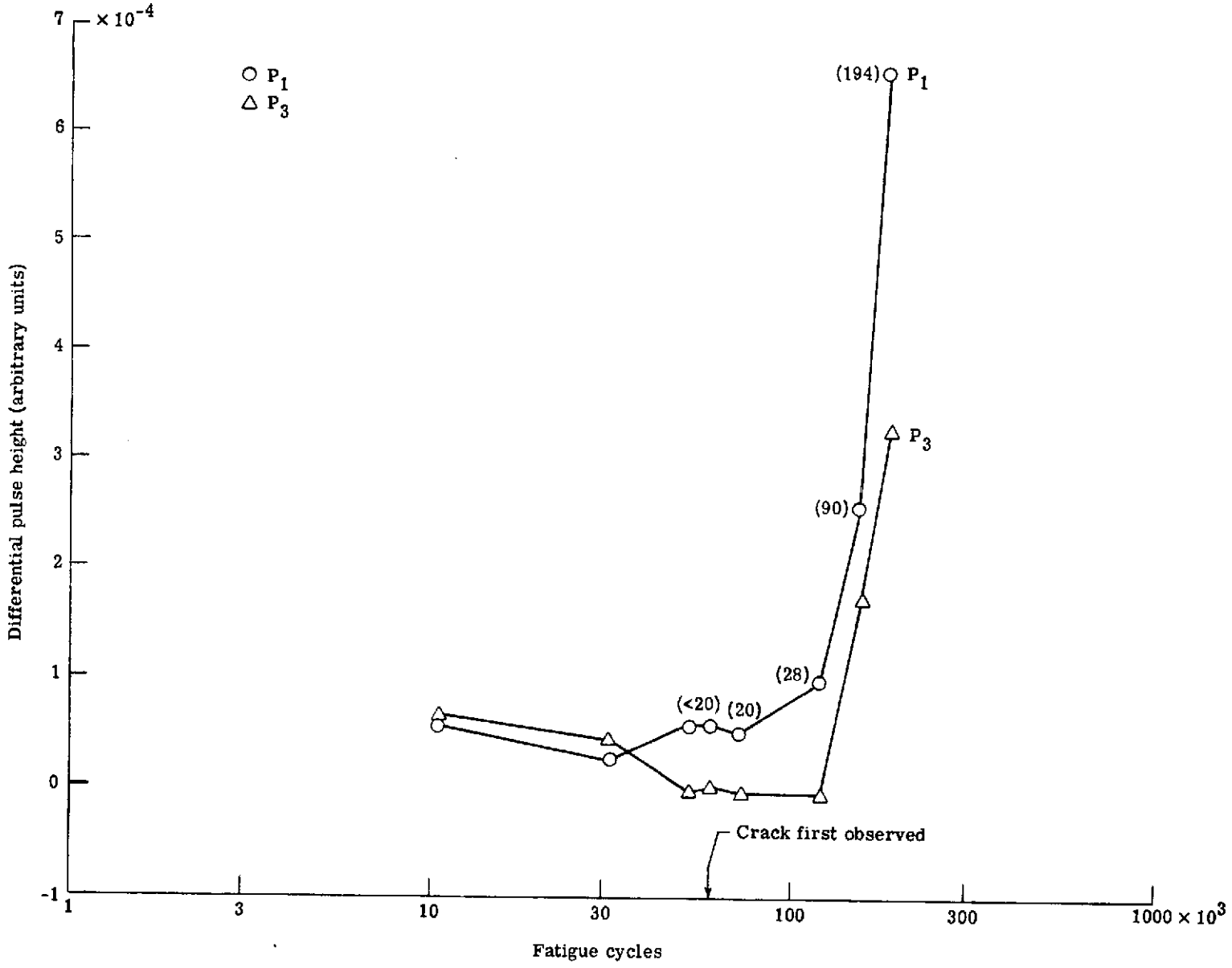

Figure 26.- Differential pulse height versus number of fatigue cycles of plate 5. Numbers in parentheses are measured crack lengths in mils.

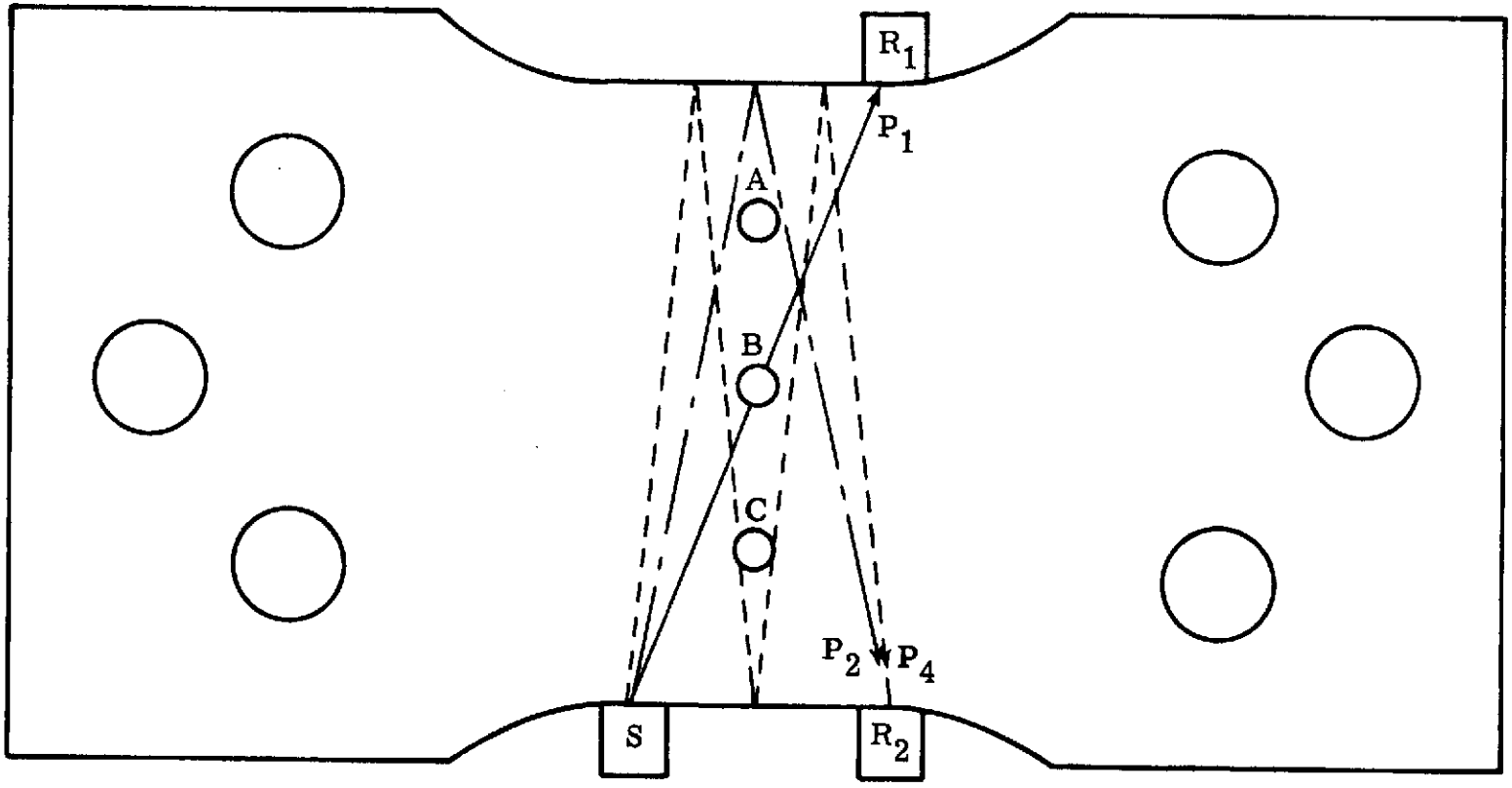

Figure 27.- Location of transducers S, R_1, and R_2, rivets A, B, and C, and grip holes in plate 8. The acoustical paths of principal pulses P_1, P_2, and P_4 are shown.

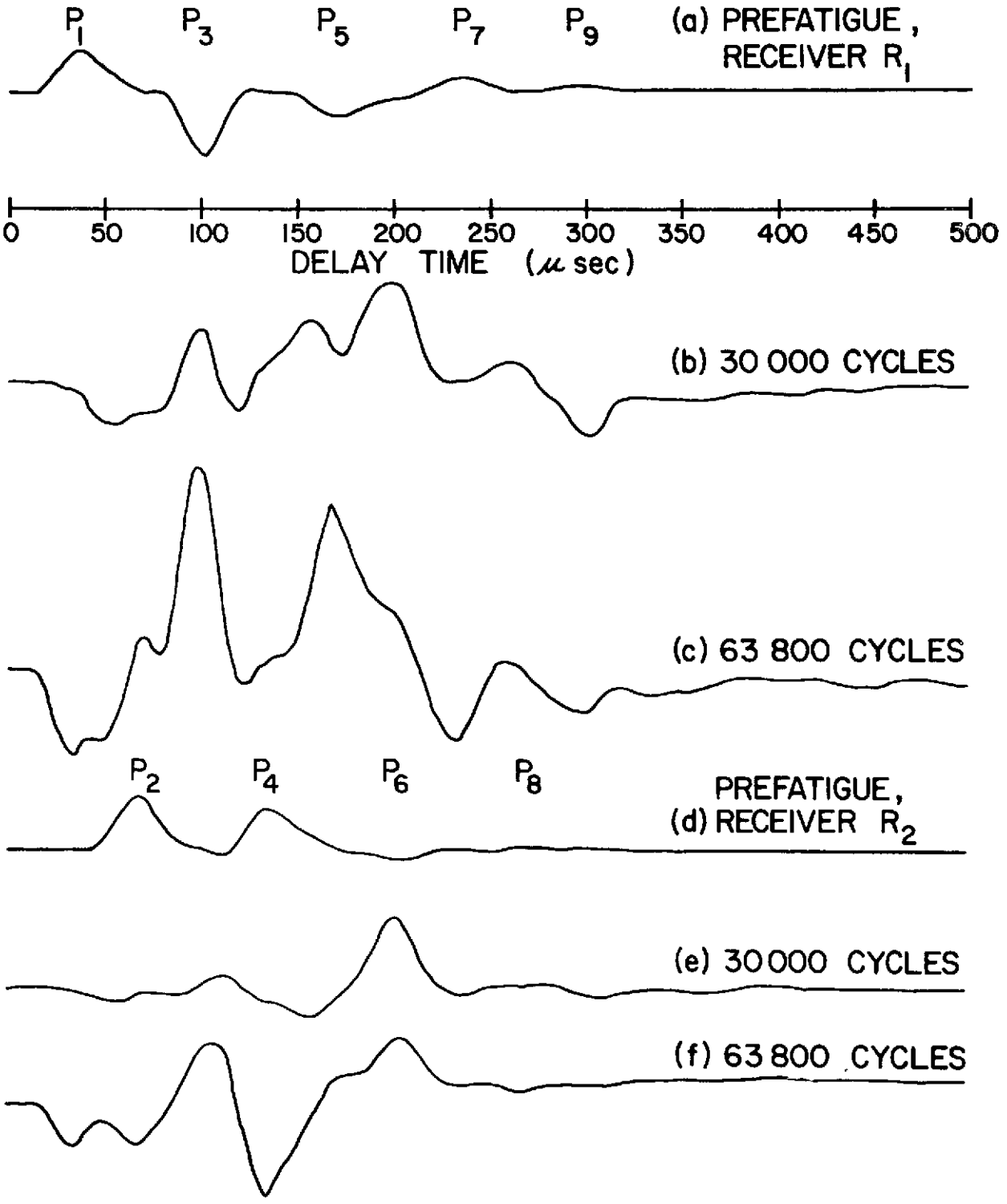

Figure 28.- Cross-correlograms of plate 8 after selected intervals of fatigue cycling: (a) reference cross-correlogram for receiver R_1 (prefatigue, scale factor = 5×10^{-3}); (b)-(c) differential cross-correlograms for R_1 (scale factor = 10^{-3}); (d) reference cross-correlogram for receiver R_2 (prefatigue, scale factor = 10^{-3}); (e)-(f) differential cross-correlograms for R_2 (scale factor = 2×10^{-3}).

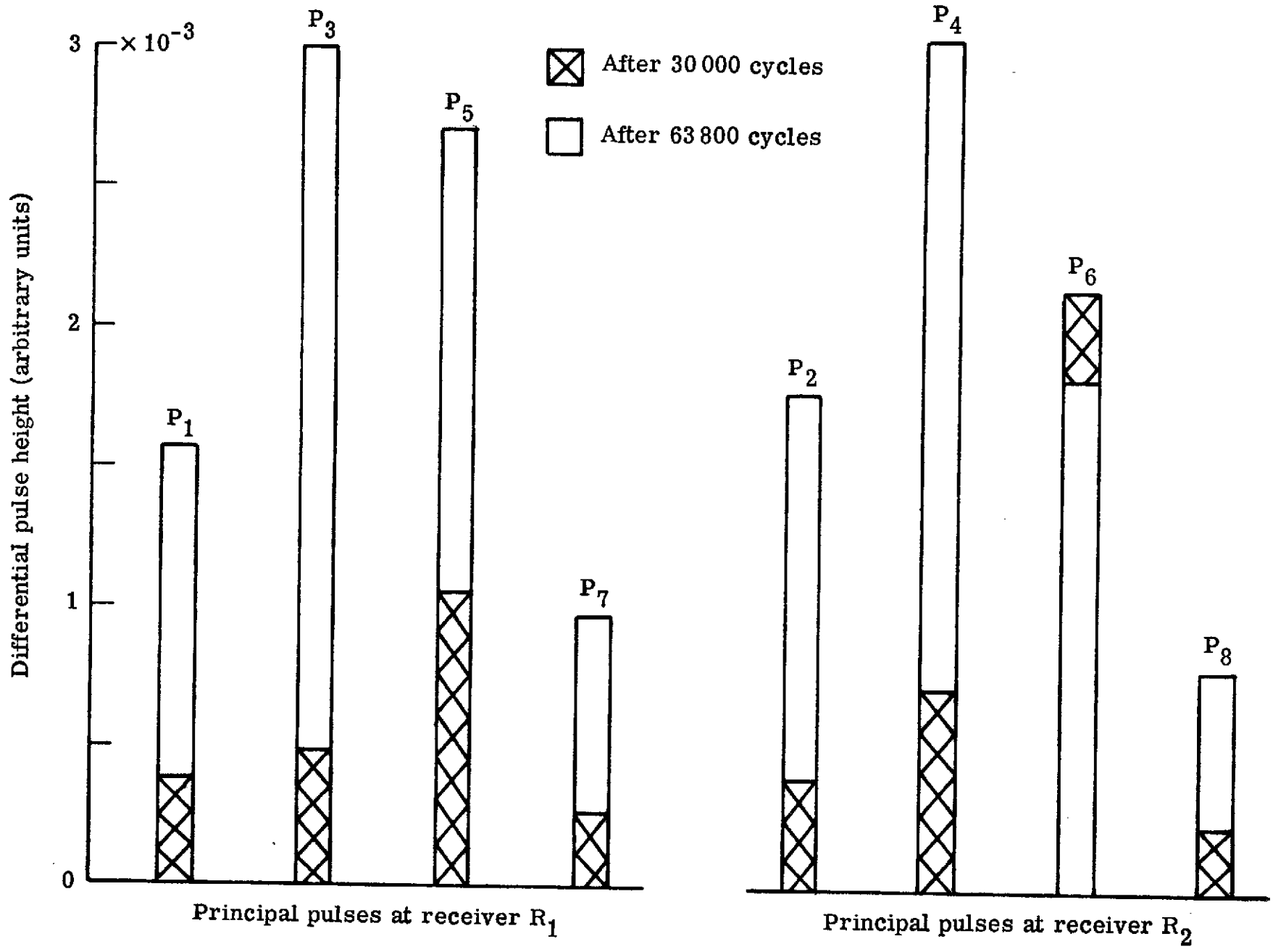

Figure 29.- Differential pulse height of principal pulses of plate 8 after 30,000 cycles and after 63,800 cycles.